Deglacial and Holocene Ssea ice and climate dynamics in the Bransfield Strait, at the Western Northern Antarctic Peninsula

Maria-Elena Vorrath[1], Juliane Müller[2,3,4], Paola Cárdenas[5], Thomas Opel[2], Sebastian Mieruch[2], Oliver Esper[2], Lester Lembke-Jene[2], Johan Etourneau[6,7], Andrea Vieth-Hillebrand[8], Niko Lahajnar[1], Carina B. Lange[5,9,10,11], Amy Leventer[12], Dimitris Evangelinos[7,13], Carlota Escutia[14], Gesine Mollenhauer[2,3]

[1]University Hamburg, Institute for Geology, Hamburg, Germany

[2]Alfred Wegener Institute, Helmholtz Centre for Polar and Marine Research, Bremerhaven, Germany

[3]MARUM – Center for Marine Environmental Sciences, University of Bremen, Germany

[4]Department of Geosciences, University of Bremen, Germany

[5]Centro de Investigación Dinámica de Ecosistemas Marinos de Altas Latitudes (IDEAL), Universidad Austral de Chile, Valdivia, Chile

[6]EPHE/PSL Research University, France

[7]UMR 5805 EPOC, CNRS, Université de Bordeaux, France

[8]Helmholtz Centre Potsdam GFZ German Research Centre for Geosciences, Potsdam, Germany

[9]Centro Oceanográfico COPAS CoastalSur-Austral/COPAS-Coastal, Universidad de Concepción, Chile

[10]Departamento de Oceanografía, Universidad de Concepción, Chile

[11]Scripps Institution of Oceanography, La Jolla, CA 92037, USA

[12]Department of Earth and Environmental GeosciencesGeology, Colgate University, New York, USA

[13]Departament de Dinàmica de la Terra i de l'Oceàn, Universitat de Barcelona, Spain

[14]Instituto Andaluz de Ciencia de la tierra, CSIC-Univ. de Granada, Spain

Correspondence to: Juliane Müller, juliane.mueller@awi.de

Abstract

The reconstruction of past sea ice distribution in the Southern Ocean is crucial for an improved understanding of ice-ocean-atmosphere feedbacks and the evaluation of Earth system and Antarctic ice sheet models. The Western Antarctic Peninsula (WAP) is experiencing rapid a warming since the start of regular monitoring of the atmospheric tempterature in since the 1950ies. Tand the associated decrease in sea ice cover contrasts the trend of

growing sea ice extent in ~~eastern~~ East Antarctica. To reveal the long-term sea ice history at the Northern Antarctic Peninsula (NAP)~~WAP~~ under changing climate conditions we examined a marine sediment core from the eastern basin of the Bransfield Strait covering the last Deglacial and the Holocene. For sea ice reconstructions, we focused on the specific sea ice biomarker lipid $IPSO_{25}$, a highly branched isoprenoid (HBI), and sea ice diatoms, whereas a phytoplankton-derived HBI triene ($C_{25:3}$) and warmer open ocean diatom assemblages reflect predominantly ice-free conditions. We further reconstruct ocean temperatures using glycerol dialkyl glycerol tetraether (GDGTs) and diatom assemblages, and compare our sea ice and temperature records with published marine sediment and ice core data. ~~Our results document a retreat of the WAP ice shelf from~~at 13.~~8~~9 ka BP ~~on (before present). A m~~Maximum ~~sea~~ ice cover is observed during ~~at 12.9 ka BP indicating~~ the Antarctic Cold Reversal (13.8 ka - 13 ka BP), while~~,~~ seasonally ice-free conditions permitting (summer) phytoplankton productivity are reconstructed for the late Deglacial and the early Holocene from 13 ka to 8.3 ka BP. ~~while a still extended but variable sea ice coverage characterized the core site during the early Holocene from 11.7 ka to 8.2 ka BP.~~ An overall decreasing sea ice trend throughout the Middle Holocene ~~is accompanied by~~coincides with ~~a successive~~ summer ocean warming and increasing phytoplankton productivity. The Late Holocene is characterized by a highly variable~~unstable~~ ~~(~~winter~~)~~ sea ice ~~cover~~concentrations~~conditions~~ and a sustained decline in~~further~~ the duration and/or concentration of spring sea ice ~~decline until 0.5 ka BP~~. Overall diverging trends in GDGT-based TEX86L and RI-OH' SOTs are found to be linked to opposing spring and summer insolation trends, respectively.

Key Words: Bransfield Strait~~Western Antarctic Peninsula~~, Holocene, sea ice cover, $IPSO_{25}$, highly branched isoprenoids, diatoms, GDGTs

1 Introduction

Sea ice significantly affects the global climate system through its impact on the atmosphere-ocean exchange of heat and gas, the physical and chemical properties of the water masses, ocean circulation, primary production and biogeochemical cycles (Chisholm, 2000; Vancoppenolle et al., 2013). Sea ice cover limits evaporation, affects precipitation and increases the reflection of solar radiation due to a high albedo (Allison et al., 1982; Butterworth and Miller, 2016; Turner et al., 2017). When sea ice forms, cold and dense brines develop, contributing to the formation of intermediate and deep waters (Nicholls et al., 2009). Importantly, the down-welling of these dense water masses can prevent warm currents from reaching the continental ~~slope~~ shelf ~~where they stimulate the basal melt~~and stimulating basal melt of Antarctic ice shelves, with implications for the stability of ice sheets and ~~eventually~~ global sea level (Cook et al., 2016; Escutia et al., 2019; Etourneau et al., 2019; Hellmer et al., 2012;

Huss and Farinotti, 2014). During the spring season, sea ice melting ~~stimulates~~ boosts marine primary production by seeding algal cells, ~~the release of~~releasing nutrients and by promoting ocean stratification and a shallow mixed layer depth (Arrigo et al., 1997; Vernet et al., 2008). In addition, nutrient supply can be locally enhanced by ~~increasing~~ wind-driven upwelling activity along the sea ice edge~~, thus triggering phytoplankton blooms~~ (Alexander and Niebauer, 1981). Enhanced carbon fixation through this ~~nutrient~~sea ice-stimulated biological pump hence leads to an increase of biological material transport and organic carbon export to the ocean floor, thus ~~contributing to lower~~lowering surface pCO_2 (Han et al., 2019; Kim et al., 2004; Schofield et al., 2018; Wefer et al., 1988).

Since satellite~~-~~-based sea-ice data became available in 1979, fast and profound changes have been observed both in the Arctic ~~and~~as well as West Antarctica ~~globally due~~and ascribed to anthropogenic global warming (IPCC, 2021). The Western Antarctic Peninsula (WAP), in particular, is experiencing a rapid warming of the atmosphere (Carrasco et al., 2021; Vaughan et al., 2003) and the ocean (Cook et al., 2016). This is~~are~~ accompanied~~is accompanied~~ by rapidly retreating glaciers and ice shelves (Cook et al., 2016; Rignot et al., 2019) and by ~~significant~~ remarkable~~remarkably~~ loss of sea ice cover in the adjacent seas (Parkinson and Cavalieri, 2012).

For an assessment of the region's past sensitivity to climate change, the deglacial and Holocene climate history of the Antarctic Peninsula (AP) has been studied extensively. The Deglacial, the transition from the Last Glacial Maximum (LGM, Clark et al., 2012) to the Holocene, is characterized by a rapid warming punctuated by a distinct cold event, the so-called Antarctic Cold Reversal (ACR) from 14.7 ka to 13 ka BP (EPICA Community Members, 2004; Mulvaney et al., 2012; Pedro et al., 2016). This drastic cooling of both atmosphere and ocean temperatures in the high Southern latitudes is well reflected in ~~recorded by~~ stable isotope records of~~s in~~ Antarctic ice cores and within marine sediments (Blunier and Brook, 2001; Domack et al., 2001; Jouzel et al., 1995; Morigi et al., 2003; Stenni et al., 2001). From the Deglacial towards the Middle Holocene, the Antarctic Peninsula Ice Sheet (APIS) retreated rapidly from the outer shelf to its modern configuration with ~~heavy~~ high melt water discharge (Bentley et al., 2014). Several ~~syntheses~~ comparisons between marine and lacustrine ~~of~~ Holocene climate records~~reflected in~~reflected from marine and lake sediment cores reveal that the timing of both hydrological and environmental changes was ~~is~~ highly variable across~~at~~ the ~~W~~AP (Allen et al., 2010; Ingólfsson et al., 2003; Minzoni et al., 2015; Roseby et al., 2022; Sjunneskog and Taylor, 2002; Totten et al., 2022).~~The ice-core records from James Ross Island (JRI) at the northeastern tip of the AP shows a pronounced warming between about 12 and 11 ka BP followed by a cooling trend until about 9 ka BP and stable temperatures until 2.5 ka BP. From 2.5 ka BP in the Late Holocene cooling was reversed since~~temperatures cooled until 0.6 ka BP (Mulvaney et al., 2012).~~ An overall consensus, however, is that WAP ocean temperatures were~~in the WAP was~~, in comparison to the Deglacial or the Late Holocene, warmer during the Early and Middle Holocene ~~Optimum~~, i.e. between 12 ka and 4 ka BP

(Shevenell et al., 2011). In contrast, marine sediment records show ~~many~~multiple different climate patterns for the Late Holocene ~~shows many different climate patterns~~ around the AP, including a continuous Neoglacial cooling (Etourneau et al., 2013)~~, whereas other records~~ other studies resolve warmer and colder phases ~~such as the Medieval Climate Anomaly and/or the Little Ice Age (Bentley et al., 2009).~~

Knowledge of past Southern Ocean sea ice variability is crucial to~~for~~ accurately model~~ling~~ climate feedbacks ~~impacting the Antarctic ice sheet stability since the LGM~~ (Crosta et al., 2022). For periods beyond the satellite era, information on past sea-ice conditions~~knowledge~~ is based on proxies from marine sediments~~, and~~ ice cores (*e.g.* Bracegirdle et al., 2015, 2019; Crosta et al., 2022; Escutia et al., 2019; Thomas et al., 2019), and snow petrel stomach oil deposits ~~-~~(McClymont et al., 2022). At present, most climate m~~M~~odels~~, however,~~ ~~do~~ not only~~often~~ fail to reproduce ~~seasonal sea ice cycles~~observed sea ice trends of the satellite era; simulated sea ice conditions~~reconstructions and observations of sea ice~~ for both glacial and interglacial periods ~~and~~ also often disagree with geological proxies (Roche et al., 2012). Ice-core based sea ice reconstructions ~~for the LGM~~ ~~are~~ primarily use ~~based on~~ the concentrations of sea salt sodium (WAIS Divide Project Members, 2015). However, since sea ~~-~~salt aerosols might be overprinted by the highly variable wind direction and meteorological conditions in Antarctica~~, and thus not reflect~~sea salt records may not sufficiently ~~be consistent in~~ reflect~~ing~~ regional sea ice conditions (Thomas et al., 2019). Although marine sediment records usually~~s mostly~~ have a lower temporal resolution than ice cores, ~~they~~ marine proxy reconstructions can resolve regional and ~~-~~ depending on the spatial distribution of sediment cores ~~- of /or~~ large-scale changes in sea ice conditions, as well as sea surface and subsurface ocean temperature, primary productivity and marine ecology (Hillaire-Marcel and de Vernal, 2007). In addition to commonly used geochemical, lithological and microfossil proxies (*e.g.* ice rafted debris (IRD), diatom assemblages, total organic carbon), new approaches focus on specific organic biomarkers - highly branched isoprenoids (HBIs) - as ~~reliable~~ proxies to distinguish between open marine and seasonally sea ice covered environments. The di-unsaturated HBI $IPSO_{25}$ (Ice Proxy for the Southern Ocean, $C_{25:2}$, Belt et al., 2016; Massé et al., 2011) that is produced by sea ice algae and deposited on the ocean floor after the sea ice melt in spring has already been applied ~~for~~ in Antarctic sea ice reconstructions (*e.g.* Barbara et al., 2013; Denis et al., 2010; Etourneau et al., 2013). Following the phytoplankton-~~P~~IP_{25}~~-~~ sea-ice index (~~,~~ PIP_{25}~~;~~) approach for the Arctic (Müller et al., 2011), $IPSO_{25}$ has been combined with phytoplankton-derived~~-~~ HBI trienes and/or sterols ~~phytoplankton~~ to determine the phytoplankton-$IPSO_{25}$ sea ice index ~~called~~ $PIPSO_{25}$ (Vorrath et al., 2019), which has been successfully evaluated with recent Antarctic spring sea ice concentrations (Lamping et al., 2021)~~.,~~ Other studies applied $PIPSO_{25}$ and examined its potential for sea ice reconstructions over ~~periods of~~ the industrial era (Vorrath et al., 2020) and ~~over~~ deglacial and Holocene time intervals in ~~has been used in paleo sea ice studies from~~ the

Formatiert: Tiefgestellt

Amundsen Sea (Lamping et al., 2020). ~~Hence, the combination to~~Ccombining these new molecular proxies with the classical diatom assemblage approach and/or geochemical ice core proxies provides~~offers~~ a thorough assessment of~~unique opportunity to robustly reconstruct~~ past sea ice conditions. ~~at the WAP.…~~

Here, we present a marine sediment record covering the past 13.8~~9~~ ka BP and ~~to~~ reconstruct Deglacial and Holocene environmental conditions in the eastern~~northern~~ Bransfield Strait at the NAP~~at the northernmost position of the WAP~~. Our study is based on a multiproxy approach focusing on the sea ice biomarker $IPSO_{25}$, an open ocean marine phytoplankton biomarker (HBI triene), and on glycerol dialkyl glycerol tetraether lipids (GDGTs) for subsurface ocean temperatures (SOT). Additional estimates~~information~~ of primary productivity, ~~about the probability of~~ winter sea ice coverage (WSI) and summer sea surface temperature (SSST) come~~s~~ from bulk sediment organic carbon and biogenic silica contents and diatom assemblages using transfer functions, respectively. In an intercomparison, we evaluate the different approaches to reconstruct sea ice conditions and ocean temperatures. ~~and~~We discuss ~~We compare discuss and compare~~ our proxy results in regard of~~with~~ other marine sediment and ice core records ~~spanning the Holocene~~ providing further insight into the environmental dynamics at the Antarctic Peninsula ~~-~~across the Deglacial and the Holocene.

2 Material and Methods

2.1 Study Area

The Bransfield Strait is located between the N~~W~~AP and the South Shetland Islands (SSI~~;) (~~Fig. 1a), comprising a trough~~t~~ (> 2000 m) ~~lying~~ between a narrow shelf to the north (SSI) and a broad shelf area to the south (AP)~~. Within this area, a shallow shelf and deeper depressions characterize the Bransfield Basin with water depths exceeding 2000 m~~ (Fig. 1b). The shelf area~~s~~ were~~as~~ affected by intense ice sheet dynamics during the last glaciation (Canals and Amblas, 2016b; Ingólfsson et al., 2003) leaving ice sheet grounding lines and glacial troughs on the sea~~-~~floor (Canals et al., 2016; Canals and Amblas, 2016a).

~~-~~ The modern Bransfield Basin is influenced by complex oceanic current systems~~.~~, ~~which are not fully constrained because three different water masses enter the basin from the east and west (Moffat and Meredith, 2018; Sangrà et al., 2011) and their mixing is not well understood. The~~ Ccold (< 0 ~~°~~C) and relatively salty Weddell Sea Water (WSW) enters from the east, flows alongshore the peninsula and fills the Bransfield Strait~~n~~ basin~~s~~ below 150 m water depth~~surface~~. ~~The WSW is also observed at greater depths (200-600 m) north of the SSI (outer shelf) and at Elephant Island due to wind driven modulation (Meijers et al., 2016).~~ In the western part of the Bransfield Strait, the WSW mixes with warmer ~~a second water mass, the~~ Bellingshausen Sea Water (BSW; 0 - 50 m water depth) and Circumpolar Deep Water (CDR; 200 - 550 m water depth; Collares et al., 2018; Sangrà

et al., 2011, 2017), which are~~is~~ transported in a branch of the Antarctic Circumpolar Current (ACC) over the Anvers Shelf. ~~It conveys well-stratified, fresh and warmer (> 0 °C) surface water~~ to a depth of about 50 m ~~(Sangrà et al., 2011). A third water mass o~~Also originating from the ACC is a third, deeper water mass, ~~O~~riginating from ~~the Circumpolar Deep Water (CDW), that is present between 200 m and 550 m (Sangrà et al., 2017). BSW and CDW flow eastward along the SSI, turn around and flow westward at the northern tip of the islands (Sangrà et al., 2011).~~ BSW and WSW form~~s~~ the ~~subsurface Bransfield front with the CDW at depth and the surface~~ Peninsula Front ~~(PF) with the WSW,~~ that runs parallel to the Antarctic mainland (Sangrà et al., 2011, 2017). The interplay of currents leads to a ~~stratification of the water column of~~pronounced pycnoclinte within the upper 20 m of the water column in summer, ~~with~~ accompanied by a steep temperature gradient in the ~~first~~ upper 100 m, as ~~below sea surface. This can be~~ observed in ~~CTD~~ hydrographic profiles from~~in~~ the Bransfield Basin that show a dominance of WSW below 200 m (see Fig. 1c and Sangrà et al., 2011). ~~The eddy system at the Peninsula Front is assumed to play a key role for mixing and upwelling of the different surface and subsurface water masses (Sangrà et al., 2011; Zhou et al., 2002), while several glaciers from the WAP influence coastal surface water due to meltwater discharge and also transport dense bottom waters to the Bransfield Basin (Meredith et al., 2018).~~

Modern sea ice conditions at the core site in the eastern Bransfield Strait are characterized by a mean winter sea ice concentration of ca. 50%, which declines to 18% and less than 2% sea ice concentration during spring and summer, respectively (*cf.* Vorrath et al., 2019). ~~Modern sea ice conditions follow a declining trend in all seasons with a nearly sea ice free summers (Hobbs et al., 2016; Vorrath et al., 2020).~~While atmospheric temperatures show a rising trend since the 1950~~ie~~s ~~ocean temperatures~~ (Carrasco et al., 2021), ocean temperatures are increasingly influenced by warm water intrusions and higher sea surface temperatures (Martinson and McKee, 2012; Meredith and King, 2005). At the core site, mean annual sea surface temperatures are -0.6 °C with up to 0.8 °C during summer (WOA 18; Boyer et al., 2018; Locarnini et al., 2018).

Primary production in the Bransfield Strait is mainly driven by mixing of water masses at the fronts (Gonçalves-Araujo et al., 2015), mixed layer depth and upwelling (Sangrà et al., 2011), sea ice dynamics (Vernet et al., 2008) and iron availability (Klunder et al., 2014). High concentrations of chlorophyll *a* and diatoms are distributed north of the ~~Peninsula Front~~PF and at the SSI, while lower production and communities of ~~nanoplanktonic~~ plankton nanoflagellates are found between the Peninsula Front and the WAP (Gonçalves-Araujo et al., 2015). Further, changes in coastal primary production are driven by upwelling, elevated iron ~~distribution~~ availability, as well as the nutrient release and surface water stratification generated by melting sea ice in the austral spring~~and the retreat of sea ice cover in spring releasing nutrients and stabilizing the water column~~ (Vernet et al., 2008). A ~~close~~ robust link between marine primary production ~~at the surface~~in surface waters and the sediment composition at the

Formatiert: Schriftart: Kursiv

underlying ocean floor is reflected in high concentrations of total organic carbon (TOC), pigments, sterols and diatoms (Cárdenas et al., 2019), and supported by studies confirming high fluxes of sinking particles (Kim et al., 2004; Wefer et al., 1988). In the study area, particle flux is highly variable with seasonal peaks occurring in late spring, which accounts for 85% of the total flux (Ducklow et al., 2008). Lithologically, the sediments consist mainly of ~~terrestrial~~ terrigenous silt and clay with varying amounts of diatom mud and ooze, and sand (Cádiz Hernández, 2019; Lamy, 2016; Wu et al., 2019).

2.2 Sediment samples and age model

Piston core PS97/072-1 (62° 0.39' S, 56° 3.86' W, 1993 m water depth, 1583 cm in length) was recovered in the eastern Bransfield Strait Basin during R/V *Polarstern* cruise PS97 (Lamy, 2016) (Fig. 1). The sediment~~core~~ is dominated by silt with thin layers of sand, clay, and traces of volcanic ash. Single pebbles are present below 630 cm. The core is disturbed~~Since we found disturbed sediments~~ below 1015 cm depth and~~,~~ we only considered samples from above this level for our analyses. S~~After an XRF scan the core s~~ampling for different analytical approaches was done at the Alfred Wegener Institute (AWI) where ~~the~~ the~~-~~ samples were stored frozen in glass vials (for biomarker analysis) and at 4 °~~-~~C in plastic bags (for micropaleontology).

The age model of core PS97/072-1 is based on ^{14}~~C~~ radiocarbon dating of eight ~~calcite~~ benthic foraminiferal and mollusk fragments samples with the mini carbon dating system (MICADAS) available at AWI (Mollenhauer et al., 2021). From the conventional ^{14}C age we subtracted a reservoir age based on modelling by Butzin et al. (2017) and also subtracted an estimated ventilation age of 1200 years to account for the considerable water depth of our site (see table supplement section 1), before we calibrated the ages with the calibration curve ~~SH~~IntCal20 (Reimer et al., 2020) ~~(Hogg et al., 2020)~~ to calendar years before present (cal BP) with Calib 7.1 (Stuiver et al., 2018). To estimate the ~~top~~ age of the core top, TOC and biogenic opal data of the piston core were matched with data from a multicore from the same sampling site that has been previously dated via ^{210}Pb (Vorrath et al., 2020; supplement section 2). Ages of sediments below the oldest radiocarbon date (868.5 cm; 12.04 ka BP) were extra~~inter~~polated assuming a constant sedimentation rate.~~AThe downcore ages between the lowest radiocarbon dates sample and the core bottom was interpolated based on previous sedimentation rates.~~ We applied the Bayesian age modelling tool *hummingage*, a freely available tool developed at AWI~~,~~ that has been successfully applied in previous studies (*e.g.* Ronge et al., 2021). As the lack of age constraints between 12 ka and 6 ka BP may introduce chronological uncertainties, we only focus on overall trends reflected in our data and refrain from detailed allocations of known climatic events in this older time period.

Formatiert: Deutsch (Deutschland)
Feldfunktion geändert
Formatiert: Deutsch (Deutschland)
Feldfunktion geändert
Formatiert: Deutsch (Deutschland)
Formatiert: Deutsch (Deutschland)
Formatiert: Deutsch (Deutschland)
Formatiert: Deutsch (Deutschland)
Feldfunktion geändert

2.3 Organic geochemical analyses of piston core PS97/072-1

For the analyses of the bulk~~several~~ organic geochemical composition~~components~~ and biomarkers, ~~the~~ 334 sediment~~s~~ samples were freeze-dried and homogenized in an agate mortar. Prior to sediment homogenization, coarse grains were separated using a sieve (5 µm mesh size). Total carbon (C) and nitrogen (N) were measured with a CNS analyzer (Elementar Vario EL III, error of standards and duplicates < 5%). TOC was measured on 0.1 g of acidified samples (500 µl HCl) and determined in a carbon-sulphur determinator (CS-800, ELTRA, standard error < 0.6%). To identify the source of TOC, measurements of stable carbon isotopes of bulk organic matter were done at Universität Hamburg (UHH), Germany, and at Washington State University (WSU), USA. At UHH, the samples were acidified three times with 100 µl 1 N HCl and dried on a hotplate. High-temperature combustion was done in an Elementar CHNOS Vario isotope elemental analyser at 950 °~~-~~C and the analysis was conducted with an Elementar IsoPrime 100 isotope ratio mass spectrometer. We calibrated the pure tank CO_2 with the International Atomic Energy Agency reference standards IAEA-CH6 and IAEA-CH7. These and two other standards (IVA Sediment and Sucrose) acted as internal standards in the measurement. The error of continuous standard duplicates was < 0.2‰ and <0.06‰ for sample duplicates. At WSU, 100 mg of freeze-dried sediment samples were used. An elemental analyzer coupled with an Isoprime isotope ratio mass spectrometer (IRMS) was used, with a precision of 0.1‰. The running standard was a protein hydrolysate calibrated against NIST standards. Isotope ratios are expressed in units per mil (‰). $\delta^{13}C$ values are expressed in ‰ against Vienna Pee Dee Belemnite (VPDB).

Biogenic opal was estimated on 327 samples following the alkaline extraction procedure described by Mortlock and Froelich (1989), but using 0.5M NaOH as a digestion solution (Müller and Schneider, 1993). Extraction and analysis by molybdate-blue spectrophotometry were conducted at the University of Concepción, Chile. Values are expressed as biogenic opal by multiplying the Si (%) by 2.4 (Mortlock and Froelich, 1989). Opal values could be ~~somewhat~~ overestimated by 2 - 2.5% since we ~~We~~ did not correct for the release of extractable Si from coexisting clay minerals~~, and thus biogenic opal values could be slightly overestimated~~ (Schlüter and Rickert, 1998). Instrumental precision was ±0.5%; error of duplicates ≤ 3%). Details on the methodology used can be found in Cárdenas et al. (2019).

The extraction, purification and identification of 137 samples to identify HBIs followed the analytical protocol published e.g. in Belt et al. (2014) and Vorrath et al. (2019). Prior to extraction, 40 µl 7-hexylnonadecane (7-HND; 0.0019 µg/µl) and 100 µl C_{46} (0.0098 µg/µl) were added~~served~~ as internal standards. Lipids were extracted using ultra sonication and a mixture of CH_2Cl_2:MeOH (v/v 2:1; 6 ml). HBIs and GDGTs were separated by means of open column chromatography using SiO_2 as the stationary phase and hexane, and CH_2Cl_2:MeOH (v/v 1:1) as

Formatiert: Nicht Hochgestellt/ Tiefgestellt

eluents. HBIs were analyzed by means of an Agilent 7890B gas chromatograph (30 m DB 1MS column, 0.25 mm diameter, 0.250 µm film thickness) coupled to an Agilent 5977B mass spectrometer (MSD, 70 eV constant ionization potential, ion source temperature 230 °C). The initial oven temperature of 60 °C was held for 3 min, ramped to 325 °C within 23 min, and was held at 325 °C for 16 min. HBIs were identified *via* comparison of their retention times (IPSO25 and HBI triene with RI 2084DB-1MS and 2046DB-1MS, respectively) and mass spectra with published mass spectra (Belt, 2018) and quantified using the ratio of peak areas of individual HBIs (*m/z* 346; *m/z* 348) and the 7-HND (*m/z* 266) standard and consideration of instrumental response factors. The error of duplicates was <1.4% for $IPSO_{25}$, <2.6% for HBI trienes. The phytoplankton-$IPSO_{25}$ index ($PIPSO_{25}$) was calculated after Vorrath et al. (2019) as:

$$PIPSO_{25} = \frac{IPSO_{25}}{IPSO_{25}+(c\times phytoplankton\ marker)} \quad . \qquad (1)$$

The concentrations of the phytoplankton-derived HBIHBI z-triene are was is considered as a phytoplankton biomarker and, since the concentrations in these samples arewere on at the same level as $IPSO_{25}$, and the c-factor was hence set to 1 (Vorrath et al., 2019). To confirm the sea-ice origin of $IPSO_{25}$, the stable carbon isotope composition of $IPSO_{25}$ was examined in 8 samples (with minimum 50 ng carbon) via GC-irm-MS at the GFZ Potsdam, Germany. The GC (7890N Agilent) equipped with an Ultra1 column (50 m x 0.2 mm diameter, 0.33 µm film thickness) was connected to a DeltaVPlus isotope ratio mass spectrometer through a modified GC-Isolink interface. Each sample was separated chromatographically usingwith a temperature program that started with an oven temperature of 80 °C, which was held for 3 min, ramped to 250 °C with 3 °C per min and then ramped to 320 °C with 5 °C per min and finally reached temperature of 325 °C with a ramp of 1 °C per min and held for 15 min. The organic substances of the GC effluent stream were oxidized to CO_2 in the combustion furnace held at 940 °C on a CuO/Ni/Pt catalyst. Samples were measured in duplicate and the standard deviation was ≤0.5 ‰. The quality of the isotope measurements was checked regularly (for each analysis) by measuring different *n*-alkane standards with known isotopic composition of n-C15, n-C20, n-C25 (in equal concentration) and n-C16 to n-C30 (in various concentrations) (provided by Campro Scientific, Germany and Arndt Schimmelmann, Indiana University, USA).

GDGTs were re-dissolved in 120 µl hexane:isopropanol (v/v 99:1) and filtered through polytetrafluoroethylene filters (0.45 µm in diameter) and analyzed using high performance liquid chromatography (HPLC, Agilent 1200 series HPLC system) coupled to a single quadrupole mass spectrometer (MS, Agilent 6120 MSD) *via* an atmospheric pressure chemical ionization (APCI) interface. The individual GDGTs were separated at 30 °C on a Prevail Cyano column (150 mm x 2.1 mm, 3µm). After injection of the sample (20 µl) it passed a 5 min isocratic elution with mobile phase A (hexane/2-propanol/chloroform; 98:1:1, flow rate 0.2 ml/min). The mobile phase B

(hexane/2-propanol/chloroform; 89:10:1) was increased to 100% in two steps: a linear increase to 10% over 20 min followed by an increase to 100% within 10 min. During the measurement, the column was cleaned after 7 min *via* backflush (5 min, flow 0.6 ml/min) and re-equilibrated with solvent A (10 min, flow 0.2 ml/min). The conditions of the APCI were a nebulizer pressure of 50 psi, vaporizer temperature and N_2 drying gas temperature 350 °C, flow 5 l/min, capillary voltage 4 kV, and corona current 5 µA. Following Liu et al. (2020), iGDGTs and br~~branched T~~the ~~-~~GDGTs were detected by selective ion monitoring (SIM) of ($M+H^+$) ions (dwell time 76 ms) using their molecular ions (GDGTs-1 (m/z 1300), GDGTs-2 (m/z 1298), GDGTs-3 (m/z 1296), crenarchaeol (m/z 1292) and GDGTs-Ia (m/z 1022), GDGTs-IIa (m/z 1036), GDGTs-IIIa (m/z 1050)) and quantified~~.~~ i~~I~~n relation to the internal standard C_{46} (*m/z* 744)~~.~~ ~~the molecular ions *m/z* of GDGTs-I (*m/z* 1300), GDGTs-II (*m/z* 1298), GDGTs-III (*m/z* 1296), and crenarchaeol (*m/z* 1292) were quantified. Also, the branched GDGTs-Ia (*m/z* 1022), GDGTs-IIa (*m/z* 1036), GDGTs-IIIa (*m/z* 1050) were quantified.~~ The hydroxylated GDGTs OH-GDGT-0 (*m/z* 1318), OH-GDGT-1 (*m/z* 1316), and OH-GDGT-2 (*m/z* 1314) were quantified in the scans of their related GDGTs (Fietz et al., 2013). The standard deviation was 0.01 units of TEX^L_{86}.

Kalanetra et al. (2009) showed that GDGT-producing Thaumarchaeota are abundant in subsurface marine waters in both Arctic and Antarctic regions. As Thaumarchaeota were found between 50 m and 200 m water depth in Antarctica (Kim et al., 2012), temperatures based on GDGTs are suggested to reflect sub-surface waters (Etourneau et al., 2013, 2019). Similarly, also RI-OH' based temperatures in Prydz Bay have been interpreted to reflect subsurface water temperatures (Liu et al., 2020). We therefore consider our results to reflect subsurface ocean temperatures (SOTs). We calculated TEX^L_{86} after Kim et al. (2012) with the *m/z* 1296~~3~~ (GDGT-3), *m/z* 1298 (GDGT-2), *m/z* 1300 (GDGT-1):

$$TEX^L_{86} = log\ log\ \left(\frac{[GDGT-2]}{[GDGT-1]+[GDGT-2]+[GDGT-3]}\right) \quad (2)$$

and calibrated with SOT = 50.8 * TEX^L_{86} + 36.1 (Kim et al., 2012). (3)

For the calculation of temperatures based on hydroxylated GDGTs we followed the approach of Lü et al. (2015)

$$RI-OH' = \frac{[OH-GDGT-1]+2\times[OH-GDGT-2]}{[OH-GDGT-0]+[OH-GDGT-1]+[OH-GDGT-2]} \quad (4)$$

and calibrated it with SOT = (RI-OH' - 0.1) / 0.0382. (5)

For the branched and isoprenoid tetraether (BIT) index for indicating terrestrial organic matter (Hopmans et al., 2004) we used crenarchaeol (m/z 1292) and the branched GDGTs and calculated it as:

$$BIT = \frac{[GDGT-Ia]+[GDGT-IIa]+[GDGT-IIIa]}{[Crenarchaeol]+[GDGT-Ia]+[GDGT-IIa]+[GDGT-IIIa]}. \quad (6)$$

2.4 Diatom analyses

We selected a set of 76 samples for the analysis of diatom assemblages. At first, sampling resolution was every 40-50 cm; thereafter, and based on the biogenic opal results, resolution was increased (every 8 cm) at intervals with high variability. ~~and then was increased~~ Freeze-dried samples (20-120 mg) were treated with hydrogen peroxide and sodium pyrophosphate to remove organic matter and clays, respectively, washed several times with DI water until reaching neutral pH. The treated samples were then settled for six hours in B-Ker2 settling chambers to promote an even distribution of settled particles (Scherer, 1994; Schrader and Gersonde, 1978; Warnock and Scherer, 2015). Once the samples were dry, the quantitative slides were mounted with Norland mounting medium (refraction index=1.56). Diatom valves per slide were counted across traverses (at least 400 valves per slide) using an Axioscop 2 Plus and Olympus BX60 at a magnification of ×1000. The counting procedure and definition of counting units followed those of Schrader and Gersonde (1978). We performed two sets of counts, with and without *Chaetoceros* resting spores. Diatoms were identified to species or species group level and, if applicable, to variety or form level following the taxonomy described by e.g., Gersonde and Zielinski (2000), Armand and Zielinski (2001), Esper et al. (2010), Esper and Gersonde (2014a, 2014b). Diatom ~~studies~~ analyses were done by the same investigator at the University of Concepción, Chile, and at Colgate University, USA.

Because diatom distribution in the Southern Ocean is directly associated with the temperature zonation and the frontal systems of the ACC (Cárdenas et al., 2019; Esper et al., 2010; Esper and Gersonde, 2014a, 2014b; Zielinski and Gersonde, 1997), diatom species were grouped into ecological assemblages reflecting i) seasonal sea ice – associated with temperatures -1.8 to 0°C; ii) cold open ocean – associated with the maximum sea-ice extent in winter and temperatures between 1 and 4°C; iii) warmer open ocean – with temperatures between 4 and 14°C, and iv) benthic-epiphytic habitats (Buffen et al., 2007; Cárdenas et al., 2019). Additionally, a group of reworked diatoms was identified ~~(supplement section 6). Diatom species were grouped into ecological assemblages reflecting i) seasonal sea ice, ii) cold open ocean, iii) warmer open ocean, and iv) benthic-epiphytic diatoms environments (Buffen et al., 2007; Cárdenas et al., 2019; Esper et al., 2010)~~ (specific group composition is described in detail in supplement section 3). ~~Additionally, a group of reworked diatoms was identified.~~ A Spearman principal component analysis (PCA) was applied to the diatom assemblages to differentiate their temporal distribution.

For estimation of winter sea ice (WSI) concentrations, we applied the transfer function MAT-D274/28/4an to the total diatom counts (including Chaetoceros resting spores). The transfer function ~~which~~ comprises 274 reference samples with 28 diatom taxa/taxa groups and considers an average of 4 analogues (Esper and Gersonde, 2014a). The analogues refer to surface sediments from the Atlantic, Pacific and western Indian sector of the Southern Ocean. There are 10 analogues from the immediate vicinity of the Antarctic Peninsula. The WSI renders sea ice

Formatiert: Englisch (Vereinigtes Königreich)

Formatiert: Englisch (Vereinigtes Königreich)

concentrations in a 1° by 1° grid for the September average of the period 1981 to 2010 (Reynolds et al., 2002, 2007). The threshold ~~of an~~between the open ocean and the~~to~~ sea ice covered area is set at 15% of sea ice concentration (Zwally et al., 2002) and the average sea ice edge is defined at 40% (Gersonde et al., 2005; Gloersen et al., 1993). ~~The qualitative estimation of sea ice concentration was derived from the abundance pattern of diatom sea-ice indicators (Gersonde and Zielinski, 2000).~~ The estimation of summer sea surface temperature (SSST) came from the transfer function IKM-D336/29/3q comprising 336 reference samples (Pacific, Atlantic and Indian Southern Ocean) with 29 diatom taxa and three factors (Esper and Gersonde, 2014b). The calculations for WSI were done with the software R (R Core Team, 2012) using the packages Vegan (Oksanen et al., 2012) and Analogue (Simpson and Oksanen, 2012).

3 Results

Based on our age model, ~~the~~ sediment core PS97/072-1 covers the last 13.8~~9~~ ka BP with a mean sedimentation rate of 67 cm/ka and a temporal resolution ranging between 50 and 150 years per sample interval. We note a higher sedimentation rate of 95 cm/ka between 5.5 ka and 3 ka BP and few short~~-term~~ intervals of ~~significantly particularly~~ lower~~ed~~ (19 cm/ka) and higher~~enhanced~~ (190 cm/ka) sedimentation (Fig. 2).

Organic geochemical bulk parameters (TOC, biogenic opal), concentrations of HBIs ($IPSO_{25}$, $C_{25:3}$ HBI triene) and diatom species of warmer open ocean conditions and sea ice assemblages of piston core PS97/072-1 are summarized in Figure 3 (additional data can be found in the supplement section ~~3~~4). TOC increases from very low values of 0.1 wt% at 13.7 ka BP to an average concentration of ~0.8 wt% between 9.9 ka BP and the top of the core with recurring short-lived minima down to 0.03 wt% during the Middle and Late Holocene (Fig. 3f). Some of these TOC minima ~~may be associated with~~occur within thin sandy layers of volcanic ash. Biogenic opal shows a similar pattern with minimum values in the lower part of the record (3.2 wt% at 13.0 ka BP) and increases throughout the Deglacial to Holocene with average values of 30 wt% and a maximum of 54.4 wt% at 5.3 ka BP (Fig. 3e).

Between 13.8~~9~~ ka and 13.4 ka BP, both $IPSO_{25}$ and HBI triene concentrations are close to or below the detection limit (0.1 µg g-1~~/g~~ OC). Throughout the record, the~~The~~ $IPSO_{25}$ concentration ranges between 0.1 to 31.5 µg g^{-1} TOC, while the concentration of the HBI triene ranges between 0.1 and 6.6 µg g^{-1} TOC (Fig. 3). $IPSO_{25}$ is absent before 13.5 ka BP and rises rapidly to maximum values of 31.5 µg g^{-1} TOC at 12.8~~9~~ ka BP. Subsequently, concentrations decrease steadily until 8.5 ka BP and then remain at~~on~~ an average level of ~4 µg g^{-1} TOC with a slightly decreasing trend to 1 µg g^{-1} TOC towards the present and smaller peaks of 10 µg g^{-1} TOC at 6.0 and 3.0 ka BP. Only traces of ~~T~~the HBI triene occur ~~at very low concentrations is largely absent~~ until 13.0 ka BP, while

its concentration ~~and~~ increases ~~to shows high elevated concentrations~~ up to 6.6 µg g^{-1} TOC after 8.5 ka BP with large fluctuations of more than 5 µg g^{-1} TOC in the Middle Holocene and from 3.4 ka BP to the present.

The diatom composition has two contrasting groups indicating open ocean conditions, a cold water assemblage and a warm~~er~~ water assemblage, and a seasonal sea ice assemblage (Fig. 3; see supplement section 3). ~~The diatom composition has two contrasting groups indicating warm open ocean conditions (Fig. 3a) and seasonal sea ice (Fig. 3c).~~ Although the group reflecting seasonal sea ice is ~~also~~ present throughout the core (mostly >20%), the highest contributions are seen before 13~~2.8~~ ka BP and ~~,~~ between 10.8 and 9.9 ka BP ~~and around 3 ka BP~~. The contribution of the warmer open ocean assemblage is very low in the Deglacial and Early Holocene, ~~and~~ rises to highest values in the Middle Holocene and remains around 10% in the Late Holocene. A biplot of a principal component analysis (PCA) shows the relationship of the ecological groups ~~along the sediment core~~for three time intervals with clear dominance of seasonal sea ~~-~~ice before 13~~.3~~ ka BP and warmer open ocean conditions after 8.5 ka BP (supplement section 5 and 6~~4~~).

Sea ice concentration estimates based on diatom assemblages (WSI) and the $PIPSO_{25}$ index as well as the content of IRD in PS97/072-1 are summarized in figure 4 (a-c). Reconstructed winter sea ice concentrations (% WSI) derived from the MAT transfer function ~~results from the diatom assemblages~~ range from 80% to 90% during the ACR and the Deglacial (13.8~~9~~ ka – 11 ka BP) and exhibit an overall decreasing trend over the Middle Holocene with ~~distinct~~ fluctuations reaching minimum sea ice concentrations of ca. 65% during the Middle and Late Holocene (Fig. 4a). $PIPSO_{25}$ values show a similar trend indicating higher sea ice cover during the ACR, the Deglacial and the Early Holocene ($PIPSO_{25}$ > 0.8) and a successive decline to 0.5 on average throughout the Middle and Late Holocene with a distinct minimum at 0.5 ka BP (Fig. 4b). IRD (lithic particles and pebbles > 5 µm) occurs frequently between 13.8~~9~~ ka and 9 ka BP and is virtually absent in the younger part of the sediment core (Fig. 4c).

Figure 5 provides ocean temperature anomalies~~reconstructions~~ based on diatom assemblages (SSST) and GDGT-derived RI-OH' and TEX_{86}^{L} SOTs in core PS97/072-1 (Fig. 5 b-d). Diatom-derived SSST estimates ~~derived from diatom data~~ generally depict~~have~~ lower~~minimum~~ temperatures ~~of -1.5 °C to 0 °C~~ during the Deglacial and Early Holocene, accompanied by ~~and~~ a shift to ca. 1 °C warm~~ering~~ temperatures ~~trend (to > 0 °C)~~ in the Middle and Late Holocene ~~with a distinct cold event at 3.1 ka BP~~ (Fig. 5b). A short cold event with a SSST decrease of ca. 1.5 °C occurred a~~t~~round 3.1 ka BP. Similar to SSSTs, ~~also~~ RI-OH'-derived SOTs likewise reflect generally lower temperatures during the Deglacial and Early Holocene, and ~~between -1.9 to -1.2 °C and a similar trend of rising~~ 0.4 °C warmer temperatures in the Middle and Late Holocene ~~to -1.2 °C until 4.2 ka BP followed by a subtle cooling to -1.4 °C~~ (Fig. 5c). TEX_{86}^{L} ~~-~~derived SOTs ~~data from GDGTs cover a temperature range of 0.7 to 3.8 °C~~

and display an opposite trend to both SSST and RI-OH' SOT with peak temperatures decreasing temperatures to 0.7 °C since from during the Deglacial and an overall Holocene cooling towards present (Fig. 5ed).

4 Discussion

4.1 The late Deglacial (13.814 ka to 11.7 ka BP)

In the oldest part of our sediment record, covering the later part of the last Deglacial from 13.814 ka until 11.7 ka BP, we observe a remarkable environmental change indicated by significant large shifts in the TOC, biomarker and diatom records (Fig. 3). TBefore 13.4 ka BP, the very low concentrations of HBIsbiomarkers (Fig. 3b and d), TOC (Fig. 3f), and biogenic opal (Fig. 3e) between 13.8 ka and 13.5 ka BP suggest that primary production of phytoplankton associated with open marine conditions and also sea ice algae synthesizing $IPSO_{25}$settings was diminished, while sea -ice related diatom species show the highest contribution of 73% (Fig. 3c), albeit with very low concentrations (supplement section see online ressource5). Highest WSI concentrations values of winter sea ice Highest (WSI, Fig. 4a) and PIPSO25 values spring sea ice ($PIPSO_{25}$, Fig. 4a, b) indicators and WSI values are pointing towards a maximum sea ice cover that lasted until summerin both seasons and are. Lowest and lowest ocean temperatures reflected in the RI-OH'-derived SOTs are well in line with peak ssNa concentrations and minimum $\delta^{18}O$ values in the EDML and, WAIS and JRI ice core records, referring to an extended sea ice cover until 13 ka BP and lowered atmospheric temperatures (Fig. 4; EPICA Community Members, 2006; Fischer et al., 2007; WAIS Divide Project Members, 2015). We note that for the interpretation of $PIPSO_{25}$ values, changes in both $IPSO_{25}$ and HBI triene concentrations need to be evaluated carefully to reliably deduce information on sea ice conditions. High $PIPSO_{25}$ values may refer to an extended sea ice cover that lasts until summer (thus hampering phytoplankton productivity/HBI triene synthesis), whereas low $PIPSO_{25}$ values point to a reduced sea ice cover in terms of duration (in spring) and/or sea ice concentration. TIn agreement with the biogenic opal and tThe near absence of $IPSO_{25}$, the HBI triene and and warm open ocean diatom species as well as minimum contents in TOC and biogenic opal between 13.89 ka and 13.5 ka BP evidences a very thick or permanent, potentially perennial sea ice cover or at least sea ice that wasis too thick to allow photosynthesis of sea ice algae inhabiting at the sea ice bottom. Similarly, Lamping et al. (2020) related the absence of $IPSO_{25}$ and a phytoplankton-derived dinosterol biomarker in sediments in the western Amundsen Sea to the re-advance of a floating ice shelf canopy during the ACR. At the PS97/072-1 core site in the eastern Bransfield Strait, both the presence of perennial sea ice, or an ice shelf tongue extending from the APIS, could explain the lack of indicators of phytoplankton productivity and $IPSO_{25}$ -synthesizing ice algae. We hence assume that the very low absolute concentrations of sea ice -associated

Formatiert: Tiefgestellt
Formatiert: Tiefgestellt
Formatiert: Tiefgestellt
Formatiert: Tiefgestellt
Formatiert: Tiefgestellt

diatoms result from lateral transport underneath the ice or reworking of sediments older than 13.5 ka BP. T~~t~~The abrupt increase in $IPSO_{25}$ concentrations at 13.5 ka BP~~, however,~~ may indicate the retreat or thinning of such an ice-~~shelf cover~~canopy, ~~from the core site~~ permitting sea ice algae growth during spring and a subsequent increase in primary production reflected in rapidly rising HBI triene concentrations since~~at~~ 13 ka BP (Fig. 3b, d). Such a transition from a perennial floating ice canopy to conditions characterized by (seasonal) sea ice cover is also reported by Milliken et al. (2009)for the nearby Maxwell Bay (King George Island; SSI) between 14 ka and 10 ka BP. Interestingly, ~~A~~a ~~significant~~ prominent decrease in sea ice associated diatoms between 13 ka and 12 ka BP (Fig. 3c)~~,~~ ~~however,~~ is not mirrored by the still high WSI concentrations. This discrepancy could relate to a weaker preservation potential of certain diatoms reflecting seasonal sea ice (e.g. Synedropsis sp., Nitzschia stellata) that are not considered within the transfer function to estimate WSI, which highlights the need to examine silica dissolution effects for the interpretation of diatom records. ~~We note that traces of biomarkers and diatoms (supplement section 4 and 65) deposited in sediments older than 13.5 ka BP may reflect sub-ice shelf lateral advection and reworking (Smith et al., 2019).~~

With regard to the ocean temperatures recorded at core site PS97/072-1, we note that the overall cool deglacial temperatures derived from diatom data (SSST) and hydroxylated GDGTs (RI-OH') seem to be linked to the lowered summer insolation (Fig. 5a), whereas higher TEX_{86}^{L} temperatures seem to be associated with a higher spring insolation (Fig. 5d). While the impact of seasonality on GDGT-based ocean temperature estimates is still under debate and would require further improvements in ~~on~~ regional calibration, the observation of maximum abundances of thaumarchaeota species (producing isoGDGTs applied to determine TEX_{86}^{L}) in Antarctic coastal waters during spring (Kalanetra et al., 2009; Murray et al., 1998) seems to support our interpretation and also helps to explain the divergent trends in TEX_{86}^{L} and RI-OH' derived SOT estimates, as the latter proxy might be also sourced by other archaea species that probably grow mostly during the summer season.

While the ACR lasts from 14.7 ka to 13 ka BP (Pedro et al., 2016) as indicated by e.g. the WAIS Divide ice core records ~~from JRI (Fig. 5h, Mulvaney et al., 2012) and WAIS Divide~~ (Fig. 5i, WAIS Divide Project Members, 2013), our sediment record shows that cold conditions with an extended sea ice cover, limiting summer phytoplankton productivity (Fig. 4a, b) ~~and reduced summer ocean temperatures~~ in the eastern Bransfield Strait, lasted until ca. 11 ka BP ~~(Figs. 4 and 5)~~. Further, the Deglacial and Early Holocene ~~(Fig. 4c)~~ IRD content (Fig. 4.c; including the presence of single large pebbles) in core PS97/072-1 points to the frequent occurrence of icebergs. ~~during the Deglacial and the Early Holocene (Fig. 4c), which relates related to~~evidencing the overall ice sheet disintegration a~~long~~t the WAP that occurred around 14 ka BP at the SSI~~South Shetland Islands~~ and promoted seasonally open-marine conditions at Anvers-Hugo Trough at 13.6 ka BP (middle WAP shelf) ~~and~~ and at 1~~2~~3.9~~2~~

ka BP in~~at~~ Palmer Deep ~~at the southern~~ (inner WAP shelf), respectively~~AP~~ (Domack et al., 2001; Domack, 2002; Jones et al., 2022; Milliken et al., 2009; Roseby et al., 2022). At our core site, rising RI-OH' SOTs~~A~~ and a slight decrease in $PIPSO_{25}$ values ~~and rising RI-OH' SOTs~~ characterize the late Deglacial between 13 ka and 11.7 ka BP (Fig. 4b, 5c). A prominent decline in large-scale sea ice cover is also reflected in the decreasing ssNA concentrations in the EDML and WAIS ice cores between 13 ka and 11.7 ka BP (Fig. 4e, f) ~~and is~~ likely related to a distinct atmospheric warming, as reflected in ice core stable water isotopes (Fig. 5h).

The ACR cooling and the subsequent Late Deglacial ~~This subsurface ocean~~ warming may relate to inter-hemispheric teleconnections through a global reorganization of atmospheric and ocean circulation that is associated with~~related to~~ the bipolar seesaw pattern of opposite climate trends between the northern and southern hemisphere (Anderson et al., 2009; Broecker, 1998; EPICA Community Members, 2006; Pedro et al., 2016). While a northward shift of the southern westerlies during the ACR (Fletcher et al., 2021) promoted Antarctic sea ice expansion and glacier readvance (potentially ~~affecting~~causing an ice cover over the PS97/072-1 core site), ~~....~~ a ~~With~~ cooling of the northern hemisphere ~~and~~with~~,~~ a southward shift of the Intertropical Convergence Zone and the southern hemisphere westerlies (Lamy et al., 2007) resulted in intensified wind stress in the Drake Passage (Timmermann et al., 2007). ~~and~~ This pattern would have increased upwelling that may have driven the continued ocean warming and sea ice retreat in Antarctica towards the Holocene (Anderson et al., 2009).

4.2 Early Holocene warming from 11.7 ka to 8.2 ka BP

The Early Holocene from 11.7 ka to 8.2 ka BP is characterized by a progressively decreasing spring sea ice cover inferred from ~~shown by~~ declining $PIPSO_{25}$ values (Fig. 4b), as well as ~~though~~ highly variable winter ~~and spring~~ sea ice cover with prominent ~~as shown by further declining WSI~~ shifts in sea ice concentration (from 90% to 65%; ~~and $PIPSO_{25}$ values~~ (Fig. 4a ~~and b~~). These WSI fluctuations are not reflected in the sea ice diatom assemblage, which, similar to the biogenic opal content, follows an increasing trend until 10.5 ka BP (Fig. 3c, e). Increased ~~Improved~~ accumulation of biogenic opal and a better preservation of (thin-walled) sea ice~~–~~related diatoms that are not used for the transfer function may explain the mismatch between the WSI record and sea ice diatom assemblage. The increase in ~~While~~ biogenic opal is further accompanied by ~~a~~ rising~~and~~ TOC content~~s exhibit increasing trends~~, while concentrations of the HBI triene and warm open ocean diatoms remain low ~~and~~, only an ~~significant~~ increase after 9 ka BP, ~~signals~~signalling~~suggests~~ higher phytoplankton productivity (Fig. 3a, b). Diatom-derived SSSTs exhibit marked fluctuations but remain relatively low until 8.2 ka BP (Fig. 5b). RI-OH' and TEX_{86}^{L} SOTs display diverging trends following the summer and spring insolation, respectively (Fig. 5).

~~Ocean temperatures based on warming is indicated by RI-OH'-based SOT, while TEX_{86}^{L} SOT and diatom-derived SSST show fluctuating temperatures without a clear trend (Fig. 5b, c and d).~~

While $PIPSO_{25}$ values display a ~~rather~~ gradual decrease in sea ice coverage, the WSI record suggests a highly variable sea ice cover, with several~~few~~ distinct sea ice minima between 11 ka and 10 ka BP and around 9 ka BP (Fig. 4a and b). These sea ice minima may have resulted from punctuated warming events, *e.g.* around~~t~~ 10 ka BP, when SSST shows a short temperature peak, which might have led to a delayed sea ice formation in autumn and winter (Fig. 5b). Another WSI minimum at 9 ka BP coincides with a major, final ~~(and final)~~ peak in IRD deposition at the core site (Fig. 4), evidencing iceberg discharge during episodes of peak AP ice-sheet ~~loss~~ retreat and enhanced calving ~~at the WAP~~ (Jones et al., 2022). As sea ice melting may have been an important driver of ~~the~~ ocean stratification, we suggest warmer, stratified surface waters with moderate production in summer, supported by increasing summer insolation ~~in December~~ (Fig. 5a). Ameliorating climate conditions, ice-shelf retreat along the NAP and the establishment of modern-like ocean conditions after 9 ka BP have also been proposed for the western Bransfield Strait ~~by (~~Heroy et al. (2008)and are well in line with the rising concentrations ~~contribution~~ of warm open ocean diatoms and the phytoplankton-derived HBI triene at our core site after 9 ka BP (Fig. 3). The general decrease in spring sea ice cover (reflected in declining $PIPSO_{25}$ values)~~Our marine records of decreasing sea ice~~ may have been fostered by~~and~~ a maximum spring and rising summer insolation (Fig. 5a, d)~~-~~, ~~and subsurface ocean temperatures~~ shortening the duration of sea ice cover. Rising RI-OH' temperatures are ~~which are~~ consistent with the overall slight warming trend recorded in the WAIS Divide ice core (Fig. 5h), which has been shown to be mainly driven by increasing summer temperatures (Jones et al., 2022). ~~…. Interestingly, neither this rise in RI-OH' derived SOTs nor the highly variable~~ The decreasing TEX_{86}^{L} SOT~~temperature~~ trend~~s~~ at core site PS97/072-1 correspond~~s~~ to the declining TEX_{86} temperatures reported for ODP site 1098 in~~at~~ Palmer Deep (Fig. 5g; Shevenell et al., 2011) though the latter displays a more pronounced temperature drop (of ca. 6 °C) between 11.7 ka and 8.2 ka BP~~.or the declining δD values recorded in the JRI ice core (Fig. 5; Mulvaney et al., 2012).~~ These regional differences may relate to changing ocean circulation patterns, ~~and~~ associated shifts in water mass distribution along~~t~~ the WAP ~~and EAP~~ and the local post-glacial environmental development during the Early Holocene. Deposition of laminated diatom oozes in the Anvers-Hugo Trough at the WAP middle shelf during the early Holocene ~~since 11.5 ka BP~~, ~~*for example*~~*e.g.*, documents episodes of extremely high productivity in response to a southward shift of the southern hemisphere westerlies and the advection of warm and nutrient-rich CDW (Roseby et al., 2022). We propose that the eastern Bransfield Strait remained mainly "inaccessible" for CDW and BSW until further ice recession between 10 ka and 5 ka BP (Ó Cofaigh et al., 2014 and references therein) permitted advection of these water masses into the Bransfield Strait. ~~We further note that the partly opposing trends~~

Formatiert: Schriftart: Kursiv

Formatiert: Schriftart: Kursiv

~~in RI-OH' and TEX_{86}^{L} temperatures at our core site could indicate that the respective GDGT producing archaea thrive in different water depths or during different seasons.~~

4.3 Middle Holocene from 8.2 ka until 4.2 ka BP

The Middle Holocene from 8.2 ka to 4.2 ka BP was~~is~~ a period of ~~significant~~ remarkable sea ice retreat and minimum iceberg ~~flux~~ activity~~records~~ at the core site indicated by decreasing WSI and $PIPSO_{25}$ values and~~,~~ virtually absent IRD (Fig. 4)~~, and an oceanic warming reflected in SSST and RI-OH' SOT (Fig. 4 and 5)~~. D~~For the whole period, d~~iatoms associated with warmer open ocean conditions, peak HBI triene concentrations and maximum TOC ~~and~~ as well as biogenic opal contents (Fig. 3) indicate~~refer to~~ a high export production during the Middle Holocene ~~(Abelmann et al., 2006; Smetacek et al., 2004)~~. Thise higher primary productivity~~export productivityproduction~~is can be linked to a decrease in~~of~~ both winter and spring sea ice ~~and potentially ice-free summers~~ indicated by WSI and $PIPSO_{25}$ minima, respectively (Fig. 4a, b)~~, and~~ elevated SSSTs and (summer) SOTs (Fig. 5b, c) promoting ice-free summer ocean conditions favorable for phytoplankton productivity. These Middle Holocene sea-ice conditions compare well with ~~the~~ modern situation at the core site characterized by a seasonal decrease in sea ice concentration from 50% during winter to mainly ice-free summers (NSIDC; Cavalieri et al., 1996)~~. like it was observed for modern sea ice conditions in this region (Vorrath et al., 2020).~~.

The continued retreat of the previously grounded APIS~~AP ice sheet~~ adjacent to~~ver~~ the Bransfield Strait between 10 ka and 5 ka BP finally opened the passage for ACC ~~surface~~ waters to enter the Bransfield Strait from the west (Bentley et al., 2014; Ó Cofaigh et al., 2014). As a result, we suggest that sea ice conditions at our core site were ~~predominantly~~ influenced by ~~branches~~ incursions of warmer oceanic waters carried~~associated~~ with~~of~~ the ACC (i.e.~~the~~ BSW and CDW) ~~leading to a shorter sea ice season and/or less intensive sea ice cover~~, while~~and~~ cold water inflow and sea ice advection from the Weddell Sea was diminished due to the still grounded ice sheet at the tip of the AP (Ó Cofaigh et al., 2014), leading to a shorter sea ice season in the eastern Bransfield Strait. This shift towards a warmer, less ice-covered ocean setting in the eastern Bransfield Strait is ~~well in line with~~reflected in the transition from proximal to distal glacimarine conditions in Maxwell Bay (Milliken et al., 2009) and may be associated with the Mid-Holocene climatic optimum. This timing contrasts the not~~a~~tion of Heroy et al. (2008), who, ~~based on diatom assemblage analyses of a sediment core in the western Bransfield Strait,~~ confined~~s~~ the Mid-Holocene climatic optimum to a shorter time interval between 6.8 ka and 5.9 ka BP based on diatom assemblage analyses of a sediment core in the western Bransfield Strait. We propose that this temporal offset may relate to regionally different responses~~, to~~ glacial retreat patterns impacting oceanic pathways and the position of frontal systems controlling primary productivity within ~~the~~ Bransfield Strait. The generally decreasing WSI and variable

$PIPSO_{25}$ values further depict different trends than $PIPSO_{25}$ values determined for the JPC10 in Palmer Deep (Fig. 4d; Etourneau et al., 2013), which suggest an overall increase in spring sea ice along the WAP until 4.2 ka BP. Though minima in spring sea ice at 7.5 ka, 6.5 ka and 5.4 ka BP at core site PS97/072-1 may be related ~~compare~~ to $PIPSO_{25}$ minima observed for JPC10, the lack of Middle Holocene age ~~constraints~~tie points in our core from the Bransfield Strait ~~deters~~prevents us from concluding on a common driver ~~causing~~for these sea ice reductions. ~~minima in spring sea ice at 6.5 ka and 5.4 ka BP The weak influence from the Weddell Sea limited the export of cold waters and supported was weak and opposite sea ice conditions were reconstructed for in the eastern AP where HBI biomarker and diatom assemblages record regionally extended sea ice cover between 7 ka and 4.5 ka BP (Fig. 4e, Barbara et al., 2016a; Minzoni et al., 2015).~~

Regarding ocean temperatures, we observe a sustained warming in RI-OH' SOT, punctuated by a cooling at 5.5 ka BP (Fig. 5c), while TEX_{86}^{L} temperatures depict a subtle cooling of ca. 0.5 ~~to 0.9~~ °C between 8.2 ka and 7 ka BP, followed by a warm reversal ~~of up to 3.1 °C~~ until 6 ka BP, and a further cooling until 4.2 ka BP (Fig. 5e). This~~A~~ Middle Holocene slight cooling trend is also~~has also been~~ observed in the TEX_{86}^{L} records~~at~~ from the core sites ~~core sites at~~ in Palmer Deep at the WAP (Fig. ~~1 and~~ 5f, g;~~,~~ Etourneau et al., 2013; Shevenell et al., 2011). The similarity between these records encourages us to assume that these TEX_{86}-derived temperatures from along the WAP and NAP are driven by spring insolation rather than ~~reflecting~~being a reflection of annual mean ocean temperature conditions ~~(see above). and contrasts a rapid warming observed in JPC38 from the eastern AP between 8 ka and 6.5 ka BP (Fig. 1 and 5, Barbara et al., 2016; Etourneau et al., 2019). Here, the near-coastal marine sediment core close to JRI (Fig. 5g, Barbara et al., 2016) records the transition from cold and heavily sea ice covered conditions at 8.2 ka BP to a warmer water environment with reduced sea ice cover permitting more phytoplankton growth between 6.5 ka and 4.2 ka BP (Barbara et al., 2016). Since stable temperatures are inferred from the JRI ice core during the entire Middle Holocene (Mulvaney et al., 2012), we suggest that the environmental changes recorded in JPC38 reflect ocean-driven rather than atmospheric processes.~~

4.4 Late Holocene and Neoglacial from 4.2 ka BP until today

The Late Holocene covering the past 4.2 ka BP is characterized by a highly variable winter sea ice and decreasing spring sea ice cover at core site PS97/072-1, as indicated ~~reflected~~ in the MAT-derived WSI and a decline in $PIPSO_{25}$ values over the past 2 ka (Fig. 4a, b). Rather constant ~~relatively stable environmental conditions at our core site reflected in constant~~ biogenic opal and TOC contents (Fig. 3e, f), however, suggest that primary productivity remained relatively unaffected by this reduction in spring sea ice cover. ~~low~~ While decreasing $IPSO_{25}$ concentrations between 2.5 ka BP and the core top (Fig. 3d) suggest a reduced productivity of the sea ice diatom

species synthesizing this molecule, no significant changes are observed in the sea ice diatom assemblage (Fig. 3c), which supports the assumption that only a restricted group of diatoms - at least *Berkeleya adeliensis* - produce $IPSO_{25}$ (Belt et al., 2016). The warm open ocean diatom assemblage follows an overall declining trend throughout the Late Holocene, which is not reflected in the highly variable and slightly increasing HBI triene concentrations (Fig. 3a, b), and a prominent decrease in HBI triene concentrations occurs only at 1 ka BP. ~~which display a slight increase until it decline and still variable but elevated HBI triene concentrations. A gradual decline in $PIPSO_{25}$ values between 4.2 ka and 1.5 ka BP contrasts the highly variable WSI concentrations (Fig. 4). …~~While the observation of cooler sea surface temperatures, and a diminished spring sea ice cover indicated by the joint decrease in the warm open ocean diatom assemblage and $PIPSO_{25}$ values since 2 ka BP may seem counterintuitive, Milliken et al. (2009) report a similar development in Maxwell Bay since 2.6 ka BP. Interestingly, records of diatom and radiolarian assemblages of a sediment core (Gebra-2) collected in ~~very~~ close vicinity to PS97/072-1 document an overall increase in sea-ice taxa over the past 3 ka BP with distinct Neoglacial events characterized by higher (denser and longer) sea ice cover (Bárcena et al., 1998). The lower sampling resolution and missing age control for the past 3 ka BP in PS97/072-1, however, hamper a more detailed comparison of diatom species in our core with those investigated for Gebra-2. The Neoglacial increase in ~~(~~spring~~)~~ sea ice cover is also indicated by a prominent rise of $PIPSO_{25}$ values determined for JPC10 in Palmer Deep (~~–~~Fig. 4d; Etourneau et al., 2013). Similarly, deposition of ssNa in the EDML ice core (Fischer et al., 2007) increases since 2 ka BP.

Minimum PS97/072-1 $PIPSO_{25}$ values at 0.5 ka BP result from~~are due~~related to ~~the significantly~~ notably reduced $IPSO_{25}$ and HBI triene concentrations (Fig. 3b, d). While ~~Similar to our observation for the Deglacial,~~ this pattern of minimum~~low~~ HBI triene and ~~minimum~~ ~~lowest~~ $IPSO_{25}$ concentrations is similar to the period between 13.8 ka and 13.5 ka BP, which was characterized by ~~, may point to perennial~~ cold conditions and a ~~heavy~~pronounced - potentially perennial - ice cover, the elevated TOC and biogenic opal values, as well as the presence of diatoms associated with warm open ocean conditions at 0.5 ka BP, point to favorable ocean conditions. We hence relate this drop in HBI concentrations to a shift in the diatom community rather than to an abrupt readvance of an ice cover.

Late Holocene ocean temperature reconstructions for core PS97/072-1 display different patterns. Generally increasing diatom-derived SSSTs are only punctuated by a cooling event at 3.1 ka BP, while RI-OH' SOT remains relatively constant with a very subtle cooling of ca. 0.2 °C between 1.5 ka and the present, which could be linked to the slight decrease in summer insolation (Fig. 5a, b, c). The decrease in TEX_{86}^{L} SOT by about 1 °C between 4 ka and 3.3 ka BP in eastern Bransfield Strait is also depicted in the TEX_{86}^{L} data from the Palmer Deep core JPC10 (~~–~~Fig. 5e, f; Etourneau et al., 2013). The following warming reflected in PS97/072-1 TEX_{86}^{L} SOT until ca. 2 ka

Formatiert: Schriftart: Kursiv

Feldfunktion geändert

Feldfunktion geändert

BP may relate to the establishment of open marine conditions fostering primary productivity at the Perseverance Drift north of Joinville Island (northern tip of the AP) as a result of warm water intrusions (Kyrmanidou et al., 2018). This warming is reversed by another cooling at about 2 ka BP - coincident with an abrupt temperature increase of ca. 4 -°C depicted in the ODP1089 TEX_{86} SOT record in Palmer Deep (-Fig. 5g; Shevenell et al., 2011). The latter~~This~~ warming is not displayed in the TEX_{86}^{L} data of the nearby JPC10 and we relate this contrast to the different approaches used to determine SOT (*i.e.*, TEX_{86} vs. TEX_{86}^{L} omitting the crenarchaeol regio-isomer, which seems to be less important for membrane adaptation in polar waters; Kim et al., 2010).

Evidently, temperature trends at the AP in the Late Holocene are highly variable between different areas (Allen et al., 2010; Barbara et al., 2016; Bárcena et al., 1998; Bentley et al., 2009; Etourneau et al., 2013; Mulvaney et al., 2012; Shevenell et al., 2011) and this is likely associated with the complex oceanographic and atmospheric settings. This heterogeneous pattern, however, contrasts with the currently observed large-scale ocean warming along the AP driven by intrusions of ACC-derived warm CDW onto the continental shelf of the WAP (Couto et al., 2017) and the NAP (Ruiz Barlett et al., 2018), as well as the overall loss of sea ice (Parkinson and Cavalieri, 2012), which supports the assumption that the changes impacting the AP already exceed natural variability.

~~conditions and the establishment of thick and/or compacted sea ice limiting the productivity of both phytoplankton and also sea ice diatoms. This short period of sea ice growth may be related to the Little Ice Age (LIA), when cooler conditions also triggered glacial readvance at the Antarctic Peninsula 500 years ago (*e.g.* Simms et al., 2021). While a significant large pulse in sea ice export from the Arctic Ocean is proposed to have caused the LIA cooling (Miles et al., 2020), knowledge about LIA sea ice conditions in the Southern Ocean is scarce and hence inconclusive (Parkinson, 1990). The Neoglacial cooling as found in the JRI ice core, for example, is clearly reflected in an increased sea ice cover at Palmer Deep since 2 ka BP (Fig. 4d, Etourneau et al., 2013) but this record, however, contains no clear evidence for a further expansion of sea ice in response to the LIA. We conclude that a comprehensive assessment of how Antarctic sea ice conditions changed during the LIA requires more studies of well-dated and ideally higher resolved sediment records.~~

~~Similar to our sea ice signals, also the Late Holocene ocean temperature reconstructions display different patterns. While RI-OH' SOT remains relatively stable, TEX_{86}^{L} indicates a cooling around 3 ka BP followed by a warming until 1.5 ka BP and another cooling towards the top of the core. Diatom-derived SSST also point to a cold period around 3 ka BP immediately followed by peaka warming peak at ca. 2.5 ka BP. Evidently, temperature trends at the WAP in the Late Holocene are highly variable between different areas (Allen et al., 2010; Barbara et al., 2016; Bárcena et al., 1998; Bentley et al., 2009; Etourneau et al., 2013; Mulvaney et al., 2012; Shevenell et al., 2011) and this may relate to the complex oceanographic and atmospheric settings. With regard to the diverging~~

Feldfunktion geändert

Feldfunktion geändert

Formatiert: Schriftart: Kursiv

temperature trends observed in sediment core PS97/072-1, we note that also inconsistencies between different analytical approaches to reconstruct ocean temperatures need to be acknowledged and examined. As previously stated, more information on the applicability and significance of GDGT-derived ocean temperatures in polar latitudes is needed.

5 Conclusions

We reconstructeded the sea ice and climate development at the Nnorthwest AP since the last Deglacial using the sediment core PS97/072-1 from the eastern Bransfield Strait. Pursuing a multi-proxy approach that focuses on organic geochemical bulk and biomarker analyses, diatom assemblage studies and transfer functions as well as IRD data, we identifiedy different Deglacial and Holocene environmental conditions impacted by sea ice and ocean temperature changes. In our multiproxy study we focused on the sea ice biomarker $IPSO_{25}$, the HBI z-triene representing open marine environments, and GDGTs for ocean temperature reconstructions. Diatom ecological groups characteristic of sea ice or cold/ warmer open ocean conditions were used, as well as diatom transfer functions to reconstruct winter sea ice and summer sea surface temperature. Additional information was derived from sedimentological records such as IRD and biogenic opal. Our results reveal the retreat of a perennial ice coverfloating ice shelf canopy after the ACR and an overall sea ice reductionretreat and summer ocean warming summer ocean temperatures during the Holocene. The late Deglacial from 13.89 ka to 11.7 ka BP was a highly dynamic period: until 13.4 ka BP primary productivitythe sedimentation of organic proxies was diminished due to a permanent ice cover during the ACR. The ACR terminated with a shift to slightly warming conditions at 13 ka BP along with a reductionretreat in the length of the spring sea ice season, which permitted phytoplankton productivity at least during summer. The Early Holocene from 11.7 ka to 8.2 ka BP was characterized by increasing summer ocean temperatureswarming, furtherslightly decreasing (in terms of duration and/or sea ice concentration) spring sea ice cover in terms of duration and/or sea ice concentration and highly variable winter sea ice cover. In the Middle Holocene from 8.2 ka to 4.2 ka BP, increased advection of BSW and CDW led to a shortened sea ice season (confined to winter and spring)ea ice coverage confined to winter and spring season stable environmental conditions prevailed with elevated and rising summer ocean temperatures fostering primary production, indicating and this period may be associated with the Middle Holocene Climatic Optimum due to intervals of lower sea ice cover. In general, sea ice seasons were short and sea ice cover was significantly greatly reduced to a minimum around 5.5 ka BP, even though high seasonal amplitudes and short-term, centennial changes in sea ice conditions occurred. During the Late Holocene, the core site experienced a distinct fluctuations invariable WSI with concentrations shifting between 90% and 60%concentration, while while $PIPSO_{25}$ values declined

continuously suggesting a less intensive or shorter spring sea ice coverspring sea ice declined continuously. and a short-term SSST cooling at 3 ka BP. Phytoplankton biomarkers as well as sea ice proxies ($IPSO_{25}$, $PIPSO_{25}$, WSI) were lowest during the period coincident with the Little Ice Age which we relate to the establishment of a multi-year sea ice cover. We note that GDGT-based TEX_{86}^{L} and RI-OH' SOTs correspond to spring and summer insolation, respectively, which may explain the divergent trends displayed by both SOT proxies. Clearly, while this observation may help with the interpretation of other Southern Ocean GDGT-based temperature estimates and the reconstruction of seasonal SOT variability, more investigations into the mechanisms driving GDGT synthesis in polar waters areis needed.

Data Availability

All data mentioned in this paper will be available at the open access repository www.pangaea.de (https://doi.pangaea.de/10.1594/PANGAEA.952279).

Author contributions

The study was conceived by MV and JM. Data collections and experimental investigations were done by MV together with CBL (core description, sampling, diatoms, biogenic opal, age model), PC (diatoms), AL (age model, diatoms), OE (diatom transfer function), GM (GDGTs ~~PS97/072-1~~, ^{14}C dating), AVH (δ^{13}C IPSO^{25}), NL (δ^{13}C TOC), LLJ (foraminifera, age model), SMS (age model, humming age), ~~CBL (core description, sampling, diatoms, biogenic opal, age model), PC (diatoms), AL (age model, diatoms), OE (diatom transfer function), GM (GDGTs PS97/072-1, ^{14}C dating), AVH (δ^{13}C IPSO$_{25}$), NL (δ^{13}C TOC),~~ JEe, DE and CE provided temperature and salinity profiles near the study site. MV drafted the manuscript. All authors contributed to the interpretation and discussion of the data and the finalization of this manuscript.

Competing interests

None of the authors have a conflict of interest.

Acknowledgement

We thank the captain, crew and chief scientist Frank Lamy of RV Polarstern cruise PS97. Denise Diekstall, Jens Hefter, Alejandro Avila and Victor Acuña are thanked for their laboratory support. We thank Helge Arz for his help with the age model. Simon Belt is acknowledged for providing the 7-HND internal standard for HBI quantification. Financial support was provided through the Helmholtz Research grant VH-NG-1101. Partial support from the Centers IDEAL (grant FONDAP 15150003) and COPAS ~~Sur-Austral~~ (grants AFB170006 and FB210021), Chile, and the Spanish Ministry of Economy, Industry and Competitivity grants CTM2017-89711-C2-½-P, co-funded by the European Union through FEDER funds, is acknowledged. We appreciate~~acknowledge~~ support by the Open Access Publication Funds of Alfred-Wegener-Institut Helmholtz-Zentrum für Polar- und Meeresforschung.

712

713

714

715

716

717

718

References

~~Abelmann, A., Gersonde, R., Cortese, G., Kuhn, G. and Smetacek, V.: Extensive phytoplankton blooms in the Atlantic sector of the glacial Southern Ocean, Paleoceanography, 21(1), 1–9, doi:10.1029/2005PA001199, 2006.~~

Alexander, V. and Niebauer, H. .: Oceanography of the eastern Bering Sea ice-edge zone in spring, Limn, 26(6), 1111–1125 [online] Available from: http://doi.wiley.com/10.1029/2007RG000250, 1981.

Allen, C. S., Oakes-Fretwell, L., Anderson, J. B. and Hodgson, D. A.: A record of Holocene glacial and oceanographic variability in Neny Fjord, Antarctic Peninsula, The Holocene, 20(4), 551–564, doi:10.1177/0959683609356581, 2010.

Allison, I., Tivendale, C. M., Akerman, G. J., Tann, J. M. and Wills, R. H.: Seasonal Variations In The Surface Energy Exchanges Over Antarctic Sea Ice and Coastal Waters, Annals of Glaciology, 3, 12–16, doi:10.3189/S0260305500002445, 1982.

Anderson, R. F., Ali, S., Bradtmiller, L. I., Nielsen, S. H. H., Fleisher, M. Q., Anderson, B. E. and Burckle, L. H.: Wind-Driven Upwelling in the Southern Ocean and the Deglacial Rise in Atmospheric CO2, Science, 323, 1443–1448, doi:10.1126/science.1167441, 2009.

Armand, L. K. and Zielinski, U.: DIATOM SPECIES OF THE GENUS *RHIZOSOLENIA* FROM SOUTHERN OCEAN SEDIMENTS: DISTRIBUTION AND TAXONOMIC NOTES, Diatom Research, 16(2), 259–294, doi:10.1080/0269249X.2001.9705520, 2001.

Arrigo, K. R., Worthen, D. L., Lizotte, M. P., Dixon, P. and Dieckmann, G.: Primary Production in Antarctic Sea Ice, Science, 276, 394–397, doi:10.1126/science.276.5311.394, 1997.

Barbara, L., Crosta, X., Schmidt, S. and Massé, G.: Diatoms and biomarkers evidence for major changes in sea ice conditions prior the instrumental period in Antarctic Peninsula, Quaternary Science Reviews, 79, 99–110, doi:10.1016/j.quascirev.2013.07.021, 2013.

Barbara, L., Crosta, X., Leventer, A., Schmidt, S., Etourneau, J., Domack, E. and Massé, G.: Environmental responses of the Northeast Antarctic Peninsula to the Holocene climate variability, Paleoceanography, 31(1), 131–147, doi:10.1002/2015PA002785, 2016.

Bárcena, M. A., Gersonde, R., Ledesma, S., Fabrés, J., Calafat, A. M., Canals, M., Sierro, F. J. and Flores, J. A.: Record of Holocene glacial oscillations in Bransfield Basin as revealed by siliceous microfossil assemblages, Antarctic Science, 10(03), 269–285, doi:10.1017/S0954102098000364, 1998.

Belt, S. T.: Source-specific biomarkers as proxies for Arctic and Antarctic sea ice, Organic Geochemistry, 125, 277–298, doi:10.1016/j.orggeochem.2018.10.002, 2018.

Belt, S. T., Smik, L., Brown, T. A., Kim, J. H., Rowland, S. J., Allen, C. S., Gal, J. K., Shin, K. H., Lee, J. I. and

Taylor, K. W. R.: Source identification and distribution reveals the potential of the geochemical Antarctic sea ice proxy IPSO25, Nature Communications, 7, 1–10, doi:10.1038/ncomms12655, 2016.

Belt, S. T. T., Brown, T. A. A., Ampel, L., Cabedo-Sanz, P., Fahl, K., Kocis, J. J. J., Massé, G., Navarro-Rodriguez, A., Ruan, J. and Xu, Y.: An inter-laboratory investigation of the Arctic sea ice biomarker proxy IP25 in marine sediments: key outcomes and recommendations, Climate of the Past, 10(1), 155–166, doi:10.5194/cp-10-155-2014, 2014.

Bentley, M. J., Hodgson, D. A., Smith, J. A., Cofaigh, C. ., Domack, E. W., Larter, R. D., Roberts, S. J., Brachfeld, S., Leventer, A., Hjort, C., Hillenbrand, C.-D. and Evans, J.: Mechanisms of Holocene palaeoenvironmental change in the Antarctic Peninsula region, The Holocene, 19(1), 51–69, doi:10.1177/0959683608096603, 2009.

Bentley, M. J., Ó Cofaigh, C., Anderson, J. B., Conway, H., Davies, B., Graham, A. G. C., Hillenbrand, C.-D., Hodgson, D. A., Jamieson, S. S. R., Larter, R. D., Mackintosh, A., Smith, J. A., Verleyen, E., Ackert, R. P., Bart, P. J., Berg, S., Brunstein, D., Canals, M., Colhoun, E. A., Crosta, X., Dickens, W. A., Domack, E., Dowdeswell, J. A., Dunbar, R., Ehrmann, W., Evans, J., Favier, V., Fink, D., Fogwill, C. J., Glasser, N. F., Gohl, K., Golledge, N. R., Goodwin, I., Gore, D. B., Greenwood, S. L., Hall, B. L., Hall, K., Hedding, D. W., Hein, A. S., Hocking, E. P., Jakobsson, M., Johnson, J. S., Jomelli, V., Jones, R. S., Klages, J. P., Kristoffersen, Y., Kuhn, G., Leventer, A., Licht, K., Lilly, K., Lindow, J., Livingstone, S. J., Massé, G., McGlone, M. S., McKay, R. M., Melles, M., Miura, H., Mulvaney, R., Nel, W., Nitsche, F. O., O'Brien, P. E., Post, A. L., Roberts, S. J., Saunders, K. M., Selkirk, P. M., Simms, A. R., Spiegel, C., Stolldorf, T. D., Sugden, D. E., van der Putten, N., van Ommen, T., Verfaillie, D., Vyverman, W., Wagner, B., White, D. A., Witus, A. E. and Zwartz, D.: A community-based geological reconstruction of Antarctic Ice Sheet deglaciation since the Last Glacial Maximum, Quaternary Science Reviews, 100(August), 1–9, doi:10.1016/j.quascirev.2014.06.025, 2014.

Blunier, T. and Brook, E. J.: Timing of millennial-scale climate change in antarctica and greenland during the last glacial period, Science, 291(5501), 109–112, doi:10.1126/science.291.5501.109, 2001.

Boyer, T., Garcia, H. E., Locarnini, R. A., Zweng, M. M., Mishonov, A. V and Reagan, J. R.: Wolrd Ocean Atlas 2018., 2018.

Bracegirdle, T. J., Stephenson, D. B., Turner, J. and Phillips, T.: The importance of sea ice area biases in 21st century multimodel projections of Antarctic temperature and precipitation, Geophysical Research Letters, 42(24), 10,832-10,839, doi:10.1002/2015GL067055, 2015.

Bracegirdle, T. J., Colleoni, F., Abram, N. J., Bertler, N. A. N., Dixon, D. A., England, M., Favier, V., Fogwill, C. J., Fyfe, J. C., Goodwin, I., Goosse, H., Hobbs, W., Jones, J. M., Keller, E. D., Khan, A. L., Phipps, S. J.,

781 Raphael, M. N., Russell, J., Sime, L., Thomas, E. R., van den Broeke, M. R. and Wainer, I.: Back to the Future:
782 Using Long-Term Observational and Paleo-Proxy Reconstructions to Improve Model Projections of Antarctic
783 Climate, Geosciences, 9(6), 255, doi:10.3390/geosciences9060255, 2019.
784 Broecker, W. S.: Paleocean circulation during the Last Deglaciation: A bipolar seesaw?, Paleoceanography,
785 13(2), 119–121, doi:10.1029/97PA03707, 1998.
786 Buffen, A., Leventer, A., Rubin, A. and Hutchins, T.: Diatom assemblages in surface sediments of the
787 northwestern Weddell Sea, Antarctic Peninsula, Marine Micropaleontology, 62(1), 7–30,
788 doi:10.1016/J.MARMICRO.2006.07.002, 2007.
789 Butterworth, B. J. and Miller, S. D.: Air-sea exchange of carbon dioxide in the Southern Ocean and Antarctic
790 marginal ice zone, Geophysical Research Letters, 43(13), 7223–7230, doi:10.1002/2016GL069581, 2016.
791 Butzin, M., Köhler, P. and Lohmann, G.: Marine radiocarbon reservoir age simulations for the past 50,000 years,
792 Geophysical Research Letters, 44(16), 8473–8480, doi:10.1002/2017GL074688, 2017.
793 Cádiz Hernández, A.: Evidencia de cambios en la productividad marina a partir de testigos sedimentarios
794 recuperados en Bahía Fildes (Maxwell Bay) y Costa de Palmer, Península Antártica durante los últimos ~ 1000
795 años, Universidad de Valparaíso., 2019.
796 Canals, M. and Amblas, D.: Seafloor kettle holes in Orleans Trough, Bransfield Basin, Antarctic Peninsula,
797 Geological Society, London, Memoirs, 46(1), 313–314, doi:10.1144/M46.16, 2016a.
798 Canals, M. and Amblas, D.: The bundle: a mega-scale glacial landform left by an ice stream, Western Bransfield
799 Basin, Geological Society, London, Memoirs, 46(1), 177–178, doi:10.1144/M46.157, 2016b.
800 Canals, M., Amblas, D. and Casamor, J. L.: Cross-shelf troughs in Central Bransfield Basin, Antarctic Peninsula,
801 Geological Society, London, Memoirs, 46(1), 171–172, doi:10.1144/M46.138, 2016.
802 Cárdenas, P., Lange, C. B., Vernet, M., Esper, O., Srain, B., Vorrath, M.-E. M.-E., Ehrhardt, S., Müller, J.,
803 Kuhn, G., Arz, H. W. H. W. H. W., Lembke-Jene, L., Lamy, F. and Paola Cárdenas, Carina B. Lange, Maria
804 Vernet, Oliver Esper, Benjamin Srain, Maria-Elena Vorrath, Sophie Ehrhardt, Juliane Müller, Gerhard Kuhn,
805 Helge W.Arz, Lester Lembke-Jene, F. L.: Biogeochemical proxies and diatoms in surface sediments across the
806 Drake Passage reflect oceanic domains and frontal systems in the region, Progress in Oceanography, 174, 72–88,
807 doi:10.1016/j.pocean.2018.10.004, 2019.
808 Carrasco, J. F., Bozkurt, D. and Cordero, R. R.: A review of the observed air temperature in the Antarctic
809 Peninsula. Did the warming trend come back after the early 21st hiatus?, Polar Science, 28, 100653,
810 doi:10.1016/j.polar.2021.100653, 2021.
811 Cavalieri, D. J., Parkinson, C. L., Gloersen, P. and Zwally, H. J.: Sea Ice Concentrations from Nimbus-7 SMMR

and DMSP SSM/I-SSMIS Passive Microwave Data, Version 1, Boulder, Colorado USA, doi:10.5067/8GQ8LZQVL0VL, 1996.

Chisholm, S. W.: Stirring times in the Southern Ocean, Nature, 407(6805), 685–686, doi:10.1038/35037696, 2000.

Clark, P. U., Shakun, J. D., Baker, P. A., Bartlein, P. J., Brewer, S., Brook, E., Carlson, A. E., Cheng, H., Kaufman, D. S., Liu, Z., Marchitto, T. M., Mix, A. C., Morrill, C., Otto-Bliesner, B. L., Pahnke, K., Russell, J. M., Whitlock, C., Adkins, J. F., Blois, J. L., Clark, J., Colman, S. M., Curry, W. B., Flower, B. P., He, F., Johnson, T. C., Lynch-Stieglitz, J., Markgraf, V., McManus, J., Mitrovica, J. X., Moreno, P. I. and Williams, J. W.: Global climate evolution during the last deglaciation, Proceedings of the National Academy of Sciences, 109(19), E1134–E1142, doi:10.1073/pnas.1116619109, 2012.

Collares, L. L., Mata, M. M., Kerr, R., Arigony-Neto, J. and Barbat, M. M.: Iceberg drift and ocean circulation in the northwestern Weddell Sea, Antarctica, Deep Sea Research Part II: Topical Studies in Oceanography, 149(January 2019), 10–24, doi:10.1016/j.dsr2.2018.02.014, 2018.

Cook, A. J., Holland, P. R., Meredith, M. P., Murray, T., Luckman, A. and Vaughan, D. G.: Ocean forcing of glacier retreat in the western Antarctic Peninsula, Science, 353(6296), 283–286, doi:10.1126/science.aae0017, 2016.

Couto, N., Martinson, D. G., Kohut, J. and Schofield, O.: Distribution of Upper Circumpolar Deep Water on the warming continental shelf of the West Antarctic Peninsula, Journal of Geophysical Research: Oceans, 122(7), 5306–5315, doi:10.1002/2017JC012840, 2017.

Crosta, X., Kohfeld, K. E., Bostock, H. C., Chadwick, M., Du Vivier, A., Esper, O., Etourneau, J., Jones, J., Leventer, A., Müller, J., Rhodes, R. H., Allen, C. S., Ghadi, P., Lamping, N., Lange, C. B., Lawler, K.-A., Lund, D., Marzocchi, A., Meissner, K. J., Menviel, L., Nair, A., Patterson, M., Pike, J., Prebble, J. G., Riesselman, C., Sadatzki, H., Sime, L. C., Shukla, S. K., Thöle, L., Vorrath, M.-E., Xiao, W. and Yang, J.: Antarctic sea ice over the past 130,000 years, Part 1: A review of what proxy records tell us, EGUsphere [preprint], doi:10.5194/egusphere-2022-99, 2022.

Denis, D., Crosta, X., Barbara, L., Massé, G., Renssen, H., Ther, O. and Giraudeau, J.: Sea ice and wind variability during the Holocene in East Antarctica: insight on middle–high latitude coupling, Quaternary Science Reviews, 29(27–28), 3709–3719, doi:10.1016/J.QUASCIREV.2010.08.007, 2010.

Domack, E., Leventer, A., Dunbar, R., Taylor, F., Brachfeld, S. and Sjunneskogs, C.: Chronology of the Palmer Deep site, Antarctic Peninsula: a Holocene palaeoenvironmental reference for the circum-Antarctic, The Holocene, 11(1), 1–9, doi:10.1191/095968301673881493, 2001.

Domack, E. W.: A Synthesis for Site 1098: Palmer Deep, in Proceedings of the Ocean Drilling Program, 178 Scientific Results, Ocean Drilling Program., 2002.

Ducklow, H. W., Erickson, M., Kelly, J., Montes-Hugo, M., Ribic, C. A., Smith, R. C., Stammerjohn, S. E. and Karl, D. M.: Particle export from the upper ocean over the continental shelf of the west Antarctic Peninsula: A long-term record, 1992–2007, Deep Sea Research Part II: Topical Studies in Oceanography, 55(18–19), 2118–2131, doi:10.1016/j.dsr2.2008.04.028, 2008.

EPICA Community Members: Eight glacial cycles from an Antarctic ice core, Nature, 429(6992), 623–628, doi:10.1038/nature02599, 2004.

EPICA Community Members: One-to-one coupling of glacial climate variability in Greenland and Antarctica, Nature, 444(7116), 195–198, doi:10.1038/nature05301, 2006.

Escutia, C., DeConto, R., Dunbar, R., De Santis, L., Shevenell, A. and Nash, T.: Keeping an Eye on Antarctic Ice Sheet Stability, Oceanography, 32(1), 32–46, doi:10.5670/oceanog.2019.117, 2019.

Esper, O. and Gersonde, R.: New tools for the reconstruction of Pleistocene Antarctic sea ice, Palaeogeography, Palaeoclimatology, Palaeoecology, 399, 260–283, doi:10.1016/J.PALAEO.2014.01.019, 2014a.

Esper, O. and Gersonde, R.: Quaternary surface water temperature estimations: New diatom transfer functions for the Southern Ocean, Palaeogeography, Palaeoclimatology, Palaeoecology, 414, 1–19, doi:10.1016/J.PALAEO.2014.08.008, 2014b.

Esper, O., Gersonde, R. and Kadagies, N.: Diatom distribution in southeastern Pacific surface sediments and their relationship to modern environmental variables, Palaeogeography, Palaeoclimatology, Palaeoecology, 287(1–4), 1–27, doi:10.1016/J.PALAEO.2009.12.006, 2010.

Etourneau, J., Collins, L. G., Willmott, V., Kim, J. H., Barbara, L., Leventer, A., Schouten, S., Sinninghe Damsté, J. S., Bianchini, A., Klein, V., Crosta, X. and Massé, G.: Holocene climate variations in the western Antarctic Peninsula: Evidence for sea ice extent predominantly controlled by changes in insolation and ENSO variability, Climate of the Past, 9(4), 1431–1446, doi:10.5194/cp-9-1431-2013, 2013.

Etourneau, J., Sgubin, G., Crosta, X., Swingedouw, D., Willmott, V., Barbara, L., Houssais, M. N., Schouten, S., Damsté, J. S. S., Goosse, H., Escutia, C., Crespin, J., Massé, G. and Kim, J. H.: Ocean temperature impact on ice shelf extent in the eastern Antarctic Peninsula, Nature Communications, 10(1), 8–15, doi:10.1038/s41467-018-08195-6, 2019.

Fietz, S., Huguet, C., Rueda, G., Hambach, B. and Rosell-Melé, A.: Hydroxylated isoprenoidal GDGTs in the Nordic Seas, Marine Chemistry, 152, 1–10, doi:10.1016/j.marchem.2013.02.007, 2013.

Fischer, H., Fundel, F., Ruth, U., Twarloh, B., Wegner, A., Udisti, R., Becagli, S., Castellano, E., Morganti, A.,

Severi, M., Wolff, E., Littot, G., Röthlisberger, R., Mulvaney, R., Hutterli, M. A., Kaufmann, P., Federer, U., Lambert, F., Bigler, M., Hansson, M., Jonsell, U., de Angelis, M., Boutron, C., Siggaard-Andersen, M.-L., Steffensen, J. P., Barbante, C., Gaspari, V., Gabrielli, P. and Wagenbach, D.: Reconstruction of millennial changes in dust emission, transport and regional sea ice coverage using the deep EPICA ice cores from the Atlantic and Indian Ocean sector of Antarctica, Earth and Planetary Science Letters, 260(1–2), 340–354, doi:10.1016/j.epsl.2007.06.014, 2007.

Fletcher, M.-S., Pedro, J., Hall, T., Mariani, M., Alexander, J. A., Beck, K., Blaauw, M., Hodgson, D. A., Heijnis, H., Gadd, P. S. and Lise-Pronovost, A.: Northward shift of the southern westerlies during the Antarctic Cold Reversal, Quaternary Science Reviews, 271, 107189, doi:10.1016/j.quascirev.2021.107189, 2021.

Gersonde, R. and Zielinski, U.: The reconstruction of late Quaternary Antarctic sea-ice distribution — the use of diatoms as a proxy for sea-ice, , 162, 263–286, doi:10.1016/S0031-0182(00)00131-0, 2000.

Gersonde, R., Crosta, X., Abelmann, A. and Armand, L.: Sea-surface temperature and sea ice distribution of the Southern Ocean at the EPILOG Last Glacial Maximum—a circum-Antarctic view based on siliceous microfossil records, Quaternary Science Reviews, 24(7–9), 869–896, doi:10.1016/J.QUASCIREV.2004.07.015, 2005.

Gloersen, P., Campbell, W. J., Cavalieri, D. J., Comiso, J. C., Parkinson, C. L. and Zwally, H. J.: Arctic and antarctic sea ice, 1978, Annals of Glaciology, 17, 149–154, 1993.

Gonçalves-Araujo, R., de Souza, M. S., Tavano, V. M. and Garcia, C. A. E.: Influence of oceanographic features on spatial and interannual variability of phytoplankton in the Bransfield Strait, Antarctica, Journal of Marine Systems, 142, 1–15, doi:10.1016/J.JMARSYS.2014.09.007, 2015.

Han, Z., Hu, C., Sun, W., Zhao, J., Pan, J., Fan, G. and Zhang, H.: Characteristics of particle fluxes in the Prydz Bay polynya, Eastern Antarctica, Science China Earth Sciences, 62(4), 657–670, doi:10.1007/s11430-018-9285-6, 2019.

Hellmer, H. H., Kauker, F., Timmermann, R., Determann, J. and Rae, J.: Twenty-first-century warming of a large Antarctic ice-shelf cavity by a redirected coastal current, Nature, 485(7397), 225–228, doi:10.1038/nature11064, 2012.

Heroy, D. C., Sjunneskog, C. and Anderson, J. B.: Holocene climate change in the Bransfield Basin, Antarctic Peninsula: evidence from sediment and diatom analysis, Antarctic Science, 20(01), 69–87, doi:10.1017/S0954102007000788, 2008.

Hillaire-Marcel, C. and de Vernal, A.: Proxies in Late Cenozoic Paleoceanography, edited by C. Hillaire-Marcel and A. de Vernal, Elsevier, Amsterdam., 2007.

Hofmann, E. E., Klinck, J. M., Lascara, C. M. and Smith, D. A.: Water mass distribution and circulation west of

the Antarctic Peninsula and including Bransfield Strait, pp. 61–80, American Geophysical Union (AGU)., 1996.

Hopmans, E. C., Weijers, J. W. H., Schefuß, E., Herfort, L., Sinninghe Damsté, J. S. and Schouten, S.: Variability in the Benguela Current upwelling system over the past 70,000 years, Earth and Planetary Science Letters, 224(1–2), 107–116, doi:10.1016/j.epsl.2004.05.012, 2004.

Huss, M. and Farinotti, D.: A high-resolution bedrock map for the Antarctic Peninsula, The Cryosphere, 8(4), 1261–1273, doi:10.5194/tc-8-1261-2014, 2014.

Ingólfsson, Ó., Hjort, C. and Humlum, O.: Glacial and Climate History of the Antarctic Peninsula since the Last Glacial Maximum, Arctic, Antarctic, and Alpine Research, 35(2), 175–186, doi:10.1657/1523-0430(2003)035[0175:GACHOT]2.0.CO;2, 2003.

IPCC: Summary for Policymakers, in Climate Change 2021_ The Physical Science Basis. Contribution of working Group I to the Sixth Assessment Report of the Intergovernmental Panel on Climate Change, edited by V. Masson-Delmotte, P. Zhai, H.-O. Pörtner, D. Roberts, J. Skea, P. R. Shukla, A. Pirani, W. Moufouma-Okia, C. Péan, R. Pidcock, S. Connors, J. B. R. Matthews, Y. Chen, X. Zhou, M. I. Gomis, E. Lonnoy, T. Maycock, M. Tignor, and T. Waterfield, p. 32, Cambridge University Press., 2021.

Jones, R. S., Johnson, J. S., Lin, Y., Mackintosh, A. N., Sefton, J. P., Smith, J. A., Thomas, E. R. and Whitehouse, P. L.: Stability of the Antarctic Ice Sheet during the pre-industrial Holocene, Nature Reviews Earth & Environment, 3(8), 500–515, doi:10.1038/s43017-022-00309-5, 2022.

Jouzel, J., Vaikmae, R., Petit, J. R., Martin, M., Duclos, Y., Stievenard, M., Lorius, C., Toots, M., Mélières, M. A., Burckle, L. H., Barkov, N. I. and Kotlyakov, V. M.: The two-step shape and timing of the last deglaciation in Antarctica, Climate Dynamics, 11(3), 151–161, doi:10.1007/BF00223498, 1995.

Kalanetra, K. M., Bano, N. and Hollibaugh, J. T.: Ammonia-oxidizing Archaea in the Arctic Ocean and Antarctic coastal waters, Environmental Microbiology, 11(9), 2434–2445, doi:10.1111/j.1462-2920.2009.01974.x, 2009.

Kim, D., Kim, D. Y., Kim, Y. J., Kang, Y. C. and Shim, J.: Downward fluxes of biogenic material in Bransfield Strait, Antarctica, Antarctic Science, 16(3), 227–237, doi:10.1017/S0954102004002032, 2004.

Kim, J.-H., van der Meer, J., Schouten, S., Helmke, P., Willmott, V., Sangiorgi, F., Koç, N., Hopmans, E. C. and Damsté, J. S. S.: New indices and calibrations derived from the distribution of crenarchaeal isoprenoid tetraether lipids: Implications for past sea surface temperature reconstructions, Geochimica et Cosmochimica Acta, 74(16), 4639–4654, doi:10.1016/j.gca.2010.05.027, 2010.

Kim, J.-H., Crosta, X., Willmott, V., Renssen, H., Bonnin, J., Helmke, P., Schouten, S. and Sinninghe Damsté, J. S.: Holocene subsurface temperature variability in the eastern Antarctic continental margin, Geophysical

Research Letters, 39(6), doi:10.1029/2012GL051157, 2012.

Klunder, M. B., Laan, P., De Baar, H. J. W., Middag, R., Neven, I. and Van Ooijen, J.: Dissolved Fe across the Weddell Sea and Drake Passage: impact of DFe on nutrient uptake, Biogeosciences, 11(3), 651–669, doi:10.5194/bg-11-651-2014, 2014.

Kyrmanidou, A., Vadman, K. J., Ishman, S. E., Leventer, A., Brachfeld, S., Domack, E. W. and Wellner, J. S.: Late Holocene oceanographic and climatic variability recorded by the Perseverance Drift, northwestern Weddell Sea, based on benthic foraminifera and diatoms, Marine Micropaleontology, 141, 10–22, doi:10.1016/j.marmicro.2018.03.001, 2018.

Lamping, N., Müller, J., Esper, O., Hillenbrand, C., Smith, J. A. and Kuhn, G.: Highly branched isoprenoids reveal onset of deglaciation followed by dynamic sea-ice conditions in the western Amundsen Sea, Antarctica, Quaternary Science Reviews, 228, 106103, doi:10.1016/j.quascirev.2019.106103, 2020.

Lamping, N., Müller, J., Hefter, J., Mollenhauer, G., Haas, C., Shi, X., Vorrath, M.-E., Lohmann, G. and Hillenbrand, C.-D.: Evaluation of lipid biomarkers as proxies for sea ice and ocean temperatures along the Antarctic continental margin, Climate of the Past, 17(5), 2305–2326, doi:10.5194/cp-17-2305-2021, 2021.

Lamy, F.: The expedition PS97 of the research vessel POLARSTERN to the Drake Passage in 2016, Reports on Polar and Marine Research, 7’01, 1–571, doi:10.2312/BzPM_0702_2016, 2016.

Lamy, F., Kaiser, J., Arz, H. W., Hebbeln, D., Ninnemann, U., Timm, O., Timmermann, A. and Toggweiler, J. R.: Modulation of the bipolar seesaw in the Southeast Pacific during Termination 1, Earth and Planetary Science Letters, 259(3–4), 400–413, doi:10.1016/j.epsl.2007.04.040, 2007.

Liu, R., Han, Z., Zhao, J., Zhang, H., Li, D., Ren, J., Pan, J. and Zhang, H.: Distribution and source of glycerol dialkyl glycerol tetraethers (GDGTs) and the applicability of GDGT-based temperature proxies in surface sediments of Prydz Bay, East Antarctica, Polar Research, 39, doi:10.33265/polar.v39.3557, 2020.

Locarnini, M., Mishonov, A., Baranova, O., Boyer, T., Zweng, M., Garcia, H., Reagan, J., Seidov, D., Weathers, K., Paver, C. and Smolyar, I.: World Ocean Atlas 2018, Volume 1: Temperature. [online] Available from: https://archimer.ifremer.fr/doc/00651/76338/, 2018.

Lü, X., Liu, X. L., Elling, F. J., Yang, H., Xie, S., Song, J., Li, X., Yuan, H., Li, N. and Hinrichs, K. U.: Hydroxylated isoprenoid GDGTs in Chinese coastal seas and their potential as a paleotemperature proxy for mid-to-low latitude marginal seas, Organic Geochemistry, 89–90, 31–43, doi:10.1016/j.orggeochem.2015.10.004, 2015.

Martinson, D. G. and McKee, D. C.: Transport of warm Upper Circumpolar Deep Water onto the western Antarctic Peninsula continental shelf, Ocean Science, 8(4), 433–442, doi:10.5194/os-8-433-2012, 2012.

967 Massé, G., Belt, S. T., Crosta, X., Schmidt, S., Snape, I., Thomas, D. N. and Rowland, S. J.: Highly branched
968 isoprenoids as proxies for variable sea ice conditions in the Southern Ocean, Antarctic Science, 23(05), 487–498,
969 doi:10.1017/S0954102011000381, 2011.
970 McClymont, E. L., Bentley, M. J., Hodgson, D. A., Spencer-Jones, C. L., Wardley, T., West, M. D., Croudace, I.
971 W., Berg, S., Gröcke, D. R., Kuhn, G., Jamieson, S. S. R., Sime, L. and Phillips, R. A.: Summer sea-ice
972 variability on the Antarctic margin during the last glacial period reconstructed from snow petrel (Pagodroma
973 nivea) stomach-oil deposits, Climate of the Past, 18(2), 381–403, doi:10.5194/cp-18-381-2022, 2022.
974 Meredith, M. P. and King, J. C.: Rapid climate change in the ocean west of the Antarctic Peninsula during the
975 second half of the 20th century, Geophysical Research Letters, 32(19), 1–5, doi:10.1029/2005GL024042, 2005.
976 Milliken, K. T., Anderson, J. B., Wellner, J. S., Bohaty, S. M. and Manley, P. L.: High-resolution Holocene
977 climate record from Maxwell Bay, South Shetland Islands, Antarctica, Geological Society of America Bulletin,
978 121(11–12), 1711–1725, doi:10.1130/B26478.1, 2009.
979 Minzoni, R. T., Anderson, J. B., Fernandez, R. and Wellner, J. S.: Marine record of Holocene climate, ocean,
980 and cryosphere interactions: Herbert Sound, James Ross Island, Antarctica, Quaternary Science Reviews, 129,
981 239–259, doi:10.1016/j.quascirev.2015.09.009, 2015.
982 Mollenhauer, G., Grotheer, H., Gentz, T., Bonk, E. and Hefter, J.: Standard operation procedures and
983 performance of the MICADAS radiocarbon laboratory at Alfred Wegener Institute (AWI), Germany, Nuclear
984 Instruments and Methods in Physics Research Section B: Beam Interactions with Materials and Atoms, 496, 45–
985 51, doi:10.1016/j.nimb.2021.03.016, 2021.
986 Morigi, C., Capotondi, L., Giglio, F., Langone, L., Brilli, M., Turi, B. and Ravaioli, M.: A possible record of the
987 Younger Dryas event in deep-sea sediments of the Southern Ocean (Pacific sector), in Palaeogeography,
988 Palaeoclimatology, Palaeoecology, vol. 198, pp. 265–278, Elsevier B.V., 2003.
989 Mortlock, R. A. and Froelich, P. N.: A simple method for the rapid determination of biogenic opal in pelagic
990 marine sediments, Deep Sea Research Part A, Oceanographic Research Papers, 36(9), 1415–1426,
991 doi:10.1016/0198-0149(89)90092-7, 1989.
992 Müller, J., Wagner, A., Fahl, K., Stein, R., Prange, M. and Lohmann, G.: Towards quantitative sea ice
993 reconstructions in the northern North Atlantic: A combined biomarker and numerical modelling approach, Earth
994 and Planetary Science Letters, 306(3–4), 137–148, doi:10.1016/J.EPSL.2011.04.011, 2011.
995 Müller, P. J. and Schneider, R.: An automated leaching method for the determination of opal in sediments and
996 particulate matter, Deep-Sea Research Part I, 40(3), 425–444, doi:https://doi.org/10.1016/0967-0637(93)90140-
997 X, 1993.

998 Mulvaney, R., Abram, N. J., Hindmarsh, R. C. A., Arrowsmith, C., Fleet, L., Triest, J., Sime, L. C., Alemany, O.
999 and Foord, S.: Recent Antarctic Peninsula warming relative to Holocene climate and ice-shelf history, Nature,
1000 489(7414), 141–144, doi:10.1038/nature11391, 2012.
1001 Murray, A. E., Preston, C. M., Massana, R., Taylor, L. T., Blakis, A., Wu, K. and DeLong, E. F.: Seasonal and
1002 Spatial Variability of Bacterial and Archaeal Assemblages in the Coastal Waters near Anvers Island, Antarctica,
1003 Applied and Environmental Microbiology, 64(7), 2585–2595, doi:10.1128/AEM.64.7.2585-2595.1998, 1998.
1004 Nicholls, K. W., Østerhus, S., Makinson, K., Gammelsrød, T. and Fahrbach, E.: Ice-ocean processes over the
1005 continental shelf of the southern Weddell Sea, Antarctica: A review, Reviews of Geophysics, 47(3), RG3003,
1006 doi:10.1029/2007RG000250, 2009.
1007 Ó Cofaigh, C., Davies, B. J., Livingstone, S. J., Smith, J. A., Johnson, J. S., Hocking, E. P., Hodgson, D. A.,
1008 Anderson, J. B., Bentley, M. J., Canals, M., Domack, E., Dowdeswell, J. A., Evans, J., Glasser, N. F.,
1009 Hillenbrand, C.-D., Larter, R. D., Roberts, S. J. and Simms, A. R.: Reconstruction of ice-sheet changes in the
1010 Antarctic Peninsula since the Last Glacial Maximum, Quaternary Science Reviews, 100, 87–110,
1011 doi:10.1016/j.quascirev.2014.06.023, 2014.
1012 Oksanen, J., Blanchet, F. G., Kindt, R., Legendre, P., Minchin, P. R., O´Hara, R. B., Simpson, G. L., Solymos,
1013 P., Stevens, M. H. H. and Wagner, H.: Vegan: Community Ecology Package (R Package Version 2.0-3), 2012.
1014 Parkinson, C. L. and Cavalieri, D. J.: Antarctic sea ice variability and trends, 1979–2010, The Cryosphere, 6,
1015 871–880, doi:10.5194/tc-6-871-2012, 2012.
1016 Pedro, J. B., Bostock, H. C., Bitz, C. M., He, F., Vandergoes, M. J., Steig, E. J., Chase, B. M., Krause, C. E.,
1017 Rasmussen, S. O., Markle, B. R. and Cortese, G.: The spatial extent and dynamics of the Antarctic Cold
1018 Reversal, Nature Geoscience, 9(1), 51–55, doi:10.1038/ngeo2580, 2016.
1019 QGIS, D. T.: QGIS Geographic Information System, [online] Available from: http://qgis.osgeo.org, 2018.
1020 R Core Team: R: a Language and Environment for Statistical Computing, R Foundation for Statistical
1021 computing, Vienna., 2012.
1022 Reimer, P. J., Austin, W. E. N., Bard, E., Bayliss, A., Blackwell, P. G., Bronk Ramsey, C., Butzin, M., Cheng,
1023 H., Edwards, R. L., Friedrich, M., Grootes, P. M., Guilderson, T. P., Hajdas, I., Heaton, T. J., Hogg, A. G.,
1024 Hughen, K. A., Kromer, B., Manning, S. W., Muscheler, R., Palmer, J. G., Pearson, C., van der Plicht, J.,
1025 Reimer, R. W., Richards, D. A., Scott, E. M., Southon, J. R., Turney, C. S. M., Wacker, L., Adolphi, F.,
1026 Büntgen, U., Capano, M., Fahrni, S. M., Fogtmann-Schulz, A., Friedrich, R., Köhler, P., Kudsk, S., Miyake, F.,
1027 Olsen, J., Reinig, F., Sakamoto, M., Sookdeo, A. and Talamo, S.: The IntCal20 Northern Hemisphere
1028 Radiocarbon Age Calibration Curve (0–55 cal kBP), Radiocarbon, 62(4), 725–757, doi:10.1017/RDC.2020.41,

2020.

Reynolds, R. W., Rayner, N. A., Smith, T. M., Stokes, D. C., Wang, W., Reynolds, R. W., Rayner, N. A., Smith, T. M., Stokes, D. C. and Wang, W.: An Improved In Situ and Satellite SST Analysis for Climate, Journal of Climate, 15(13), 1609–1625, doi:10.1175/1520-0442(2002)015<1609:AIISAS>2.0.CO;2, 2002.

Reynolds, R. W., Smith, T. M., Liu, C., Chelton, D. B., Casey, K. S., Schlax, M. G., Reynolds, R. W., Smith, T. M., Liu, C., Chelton, D. B., Casey, K. S. and Schlax, M. G.: Daily High-Resolution-Blended Analyses for Sea Surface Temperature, Journal of Climate, 20(22), 5473–5496, doi:10.1175/2007JCLI1824.1, 2007.

Rignot, E., Mouginot, J., Scheuchl, B., van den Broeke, M., van Wessem, M. J. and Morlighem, M.: Four decades of Antarctic Ice Sheet mass balance from 1979–2017, Proceedings of the National Academy of Sciences, 116(4), 1095–1103, doi:10.1073/pnas.1812883116, 2019.

Roche, D. M., Crosta, X. and Renssen, H.: Evaluating Southern Ocean sea-ice for the Last Glacial Maximum and pre-industrial climates: PMIP-2 models and data evidence, Quaternary Science Reviews, 56, 99–106, doi:10.1016/j.quascirev.2012.09.020, 2012.

Ronge, T. A., Lippold, J., Geibert, W., Jaccard, S. L., Mieruch-Schnülle, S., Süfke, F. and Tiedemann, R.: Deglacial patterns of South Pacific overturning inferred from 231Pa and 230Th, Scientific Reports, 11(1), doi:10.1038/s41598-021-00111-1, 2021.

Roseby, Z. A., Smith, J. A., Hillenbrand, C.-D., Cartigny, M. J. B., Rosenheim, B. E., Hogan, K. A., Allen, C. S., Leventer, A., Kuhn, G., Ehrmann, W. and Larter, R. D.: History of Anvers-Hugo Trough, western Antarctic Peninsula shelf, since the Last Glacial Maximum. Part I: Deglacial history based on new sedimentological and chronological data, Quaternary Science Reviews, 291, 107590, doi:10.1016/j.quascirev.2022.107590, 2022.

Ruiz Barlett, E. M., Tosonotto, G. V., Piola, A. R., Sierra, M. E. and Mata, M. M.: On the temporal variability of intermediate and deep waters in the Western Basin of the Bransfield Strait, Deep Sea Research Part II: Topical Studies in Oceanography, 149, 31–46, doi:10.1016/j.dsr2.2017.12.010, 2018.

Sangrà, P., Gordo, C., Hernández-Arencibia, M., Marrero-Díaz, A., Rodríguez-Santana, A., Stegner, A., Martínez-Marrero, A., Pelegrí, J. L. and Pichon, T.: The Bransfield current system, Deep Sea Research Part I: Oceanographic Research Papers, 58(4), 390–402, doi:10.1016/J.DSR.2011.01.011, 2011.

Sangrà, P., Stegner, A., Hernández-Arencibia, M., Marrero-Díaz, Á., Salinas, C., Aguiar-González, B., Henríquez-Pastene, C. and Mouriño-Carballido, B.: The Bransfield Gravity Current, Deep-Sea Research Part I: Oceanographic Research Papers, 119(November 2016), 1–15, doi:10.1016/j.dsr.2016.11.003, 2017.

Scherer, R. P.: A new method for the determination of absolute abundance of diatoms and other silt-sized sedimentary particles, Journal of Paleolimnology, 12(2), 171–179, doi:10.1007/BF00678093, 1994.

Schlüter, M. and Rickert, D.: Effect of pH on the measurement of biogenic silica, Marine Chemistry, 63(1–2), 81–92, doi:10.1016/S0304-4203(98)00052-8, 1998.

Schofield, O., Brown, M., Kohut, J., Nardelli, S., Saba, G., Waite, N. and Ducklow, H.: Changes in the upper ocean mixed layer and phytoplankton productivity along the West Antarctic Peninsula, Philosophical Transactions of the Royal Society A: Mathematical, Physical and Engineering Sciences, 376(2122), doi:10.1098/rsta.2017.0173, 2018.

Schrader, H. and Gersonde, R.: Diatoms and silicoflagellates, in Micropaleontological Methods and Techniques - An Excercise on an Eight Meter Section of the Lower Pliocene of Capo Rossello, Sicily, Utrecht Micropaleontological Bulletins, vol. 17, edited by W. J. Zachariasse, W. R. Riedel, A. Sanfilippo, R. R. Schmidt, M. J. Brolsma, H. J. Schrader, R. Gersonde, M. M. Drooger, and J. A. Broekman, pp. 129–176., 1978.

Shevenell, A. E., Ingalls, A. E., Domack, E. W. and Kelly, C.: Holocene Southern Ocean surface temperature variability west of the Antarctic Peninsula, Nature, 470(7333), 250–254, doi:10.1038/nature09751, 2011.

Simpson, G. L. and Oksanen, J.: Analogue: Analogue Matching and Modern Analogue Technique Transfer Function Models. R Package Version 0.8-2, 2012.

Sjunneskog, C. and Taylor, F.: Postglacial marine diatom record of the Palmer Deep, Antarctic Peninsula (ODP Leg 178, Site 1098) 1. Total diatom abundance, Paleoceanography, 17(3), PAL 4-1-PAL 4-8, doi:10.1029/2000PA000563, 2002.

Stenni, B., Masson-Delmotte, V., Johnsen, S., Jouzel, J., Longinelli, A., Monnin, E., Röthlisberger, R. and Selmo, E.: An Oceanic Cold Reversal During the Last Deglaciation, Science, 293(5537), 2074–2077, doi:10.1126/science.1059702, 2001.

Stuiver, M., Reimer, P. J. and Reimer, R. W.: Calib 7.1, [online] Available from: http://calib.org/ (Accessed 20 November 2021), 2018.

Thomas, Allen, Etourneau, King, Severi, Winton, Mueller, Crosta and Peck: Antarctic Sea Ice Proxies from Marine and Ice Core Archives Suitable for Reconstructing Sea Ice over the past 2000 Years, Geosciences, 9(12), 506, doi:10.3390/geosciences9120506, 2019.

Timmermann, A., Okumura, Y., An, S.-I., Clement, A., Dong, B., Guilyardi, E., Hu, A., Jungclaus, J. H., Renold, M., Stocker, T. F., Stouffer, R. J., Sutton, R., Xie, S.-P. and Yin, J.: The Influence of a Weakening of the Atlantic Meridional Overturning Circulation on ENSO, Journal of Climate, 20(19), 4899–4919, doi:10.1175/JCLI4283.1, 2007.

Totten, R. L., Fonseca, A. N. R., Wellner, J. S., Munoz, Y. P., Anderson, J. B., Tobin, T. S. and Lehrmann, A. A.: Oceanographic and climatic influences on Trooz Glacier, Antarctica during the Holocene, Quaternary

Science Reviews, 276, 107279, doi:10.1016/j.quascirev.2021.107279, 2022.

Turner, J., Orr, A., Gudmundsson, G. H., Jenkins, A., Bingham, R. G., Hillenbrand, C.-D. and Bracegirdle, T. J.: Atmosphere-ocean-ice interactions in the Amundsen Sea Embayment, West Antarctica, Reviews of Geophysics, 55(1), 235–276, doi:10.1002/2016RG000532, 2017.

Vancoppenolle, M., Meiners, K. M., Michel, C., Bopp, L., Brabant, F., Carnat, G., Delille, B., Lannuzel, D., Madec, G., Moreau, S., Tison, J. L. and van der Merwe, P.: Role of sea ice in global biogeochemical cycles: Emerging views and challenges, Quaternary Science Reviews, 79, 207–230, doi:10.1016/j.quascirev.2013.04.011, 2013.

Vaughan, D. G., Marshall, G. J., Connolley, W. M., Parkinson, C., Mulvaney, R., Hodgson, D. A., King, J. C., Pudsey, C. J. and Turner, J.: Recent Rapid Regional Climate Warming on the Antarctic Peninsula, Climatic Change, 60(3), 243–274, doi:10.1023/A:1026021217991, 2003.

Vernet, M., Martinson, D., Iannuzzi, R., Stammerjohn, S., Kozlowski, W., Sines, K., Smith, R. and Garibotti, I.: Primary production within the sea-ice zone west of the Antarctic Peninsula: I—Sea ice, summer mixed layer, and irradiance, Deep Sea Research Part II: Topical Studies in Oceanography, 55(18–19), 2068–2085, doi:10.1016/j.dsr2.2008.05.021, 2008.

Vorrath, M.-E., Müller, J., Esper, O., Mollenhauer, G., Haas, C., Schefuß, E. and Fahl, K.: Highly branched isoprenoids for Southern Ocean sea ice reconstructions: a pilot study from the Western Antarctic Peninsula, Biogeosciences, 16(15), 2961–2981, doi:10.5194/bg-16-2961-2019, 2019.

Vorrath, M.-E., Müller, J., Rebolledo, L., Cárdenas, P., Shi, X., Esper, O., Opel, T., Geibert, W., Muñoz, P., Haas, C., Kuhn, G., Lange, C. B., Lohmann, G. and Mollenhauer, G.: Sea ice dynamics in the Bransfield Strait, Antarctic Peninsula, during the past 240 years: a multi-proxy intercomparison study, Climate of the Past, 16(6), 2459–2483, doi:10.5194/cp-16-2459-2020, 2020.

WAIS Divide Project Members: Onset of deglacial warming in West Antarctica driven by local orbital forcing, Nature, 500(7463), 440–444, doi:10.1038/nature12376, 2013.

WAIS Divide Project Members: Precise interpolar phasing of abrupt climate change during the last ice age, Nature, 520(7549), 661–665, doi:10.1038/nature14401, 2015.

Warnock, J. P. and Scherer, R. P.: A revised method for determining the absolute abundance of diatoms, Journal of Paleolimnology, 53(1), 157–163, doi:10.1007/s10933-014-9808-0, 2015.

Wefer, G., Fischer, G., Füetterer, D. and Gersonde, R.: Seasonal particle flux in the Bransfield Strait, Antartica, Deep Sea Research Part A. Oceanographic Research Papers, 35(6), 891–898, doi:10.1016/0198-0149(88)90066-0, 1988.

Wu, S., Kuhn, G., Diekmann, B., Lembke-Jene, L., Tiedemann, R., Zheng, X., Ehrhardt, S., Arz, H. W. and Lamy, F.: Surface sediment characteristics related to provenance and ocean circulation in the Drake Passage sector of the Southern Ocean, Deep Sea Research Part I: Oceanographic Research Papers, 154, 103135, doi:10.1016/j.dsr.2019.103135, 2019.

Zielinski, U. and Gersonde, R.: Diatom distribution in Southern Ocean surface sediments (Atlantic sector): Implications for paleoenvironmental reconstructions, Palaeogeography, Palaeoclimatology, Palaeoecology, 129(3–4), 213–250, doi:10.1016/S0031-0182(96)00130-7, 1997.

Zwally, H. J., Comiso, J. C., Parkinson, C. L., Cavalieri, D. J. and Gloersen, P.: Variability of Antarctic sea ice 1979–1998, Journal of Geophysical Research, 107(C5), 3041, doi:10.1029/2000JC000733, 2002.

Figures

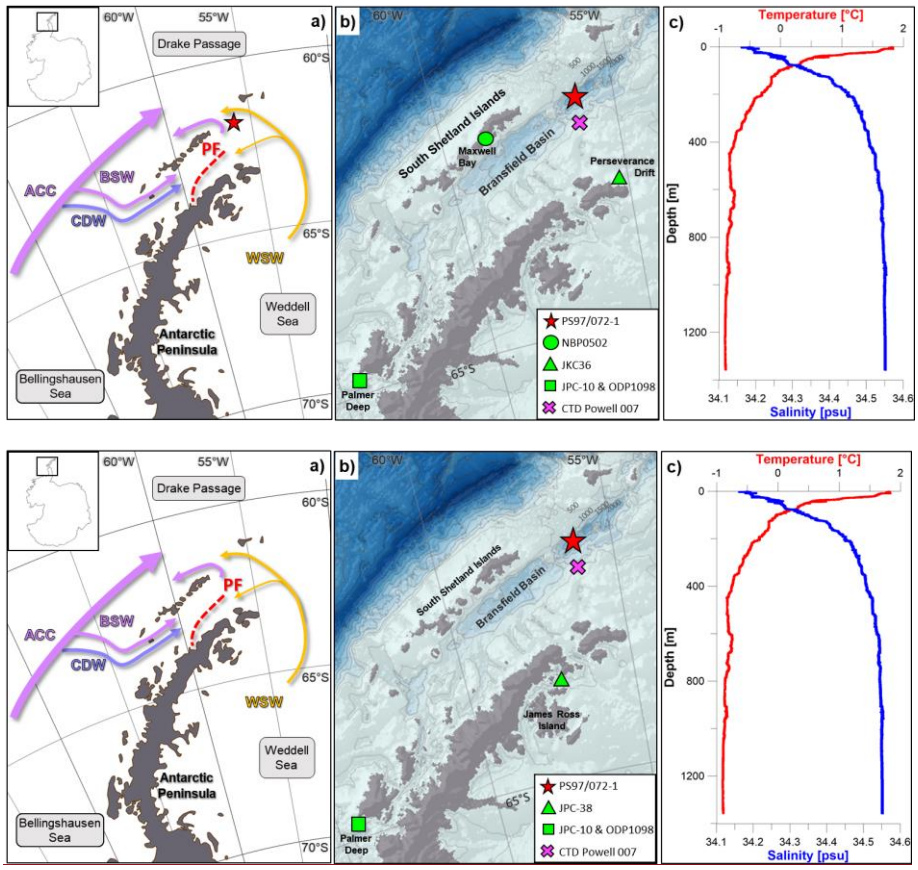

Figure 1: a) Overview map with modern oceanography in the study area (Hofmann et al., 1996; Sangrà et al., 2011). ACC = Antarctic Circumpolar Current, BSW = Bellingshausen Sea Water, CDW = Circumpolar Deep Water, WSW = Weddell Sea Water, and PF = Peninsula Front. b) Bathymetric features in the Bransfield Strait with the location of sediment core PS97/072-1 (red star) and other sediment records discussed in the text (green), and the CTD station (purple cross) where c) the vertical profile of ocean temperature and salinity (cruise POWELL2020, CTD 007 (62°09.075'S, 56°37.09'W) from 27.01.2020) shows a clear stratification of the upper 100 m of the water column. It indicates that surface waters are dominated by the BSW, while the basin is filled with WSW water. Maps were done with QGIS 3.0 (QGIS, 2018)and the bathymetry was taken from GEBCO_14 from 2015.

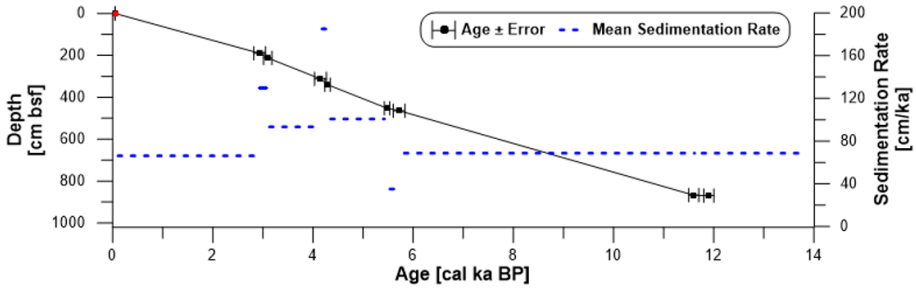

Figure 2: Age-depth model for sediment core PS97/072-1 based on eight ^{14}C dated calcite samples (black) with error bars and mean sedimentation rates (cm/ka, dashed blue line). The core top age (red) was estimated as 0.05 ka BP from matching with the ^{210}Pb-dated multicore PS97/072-2 (Vorrath et al., 2020; see supplement section 2).

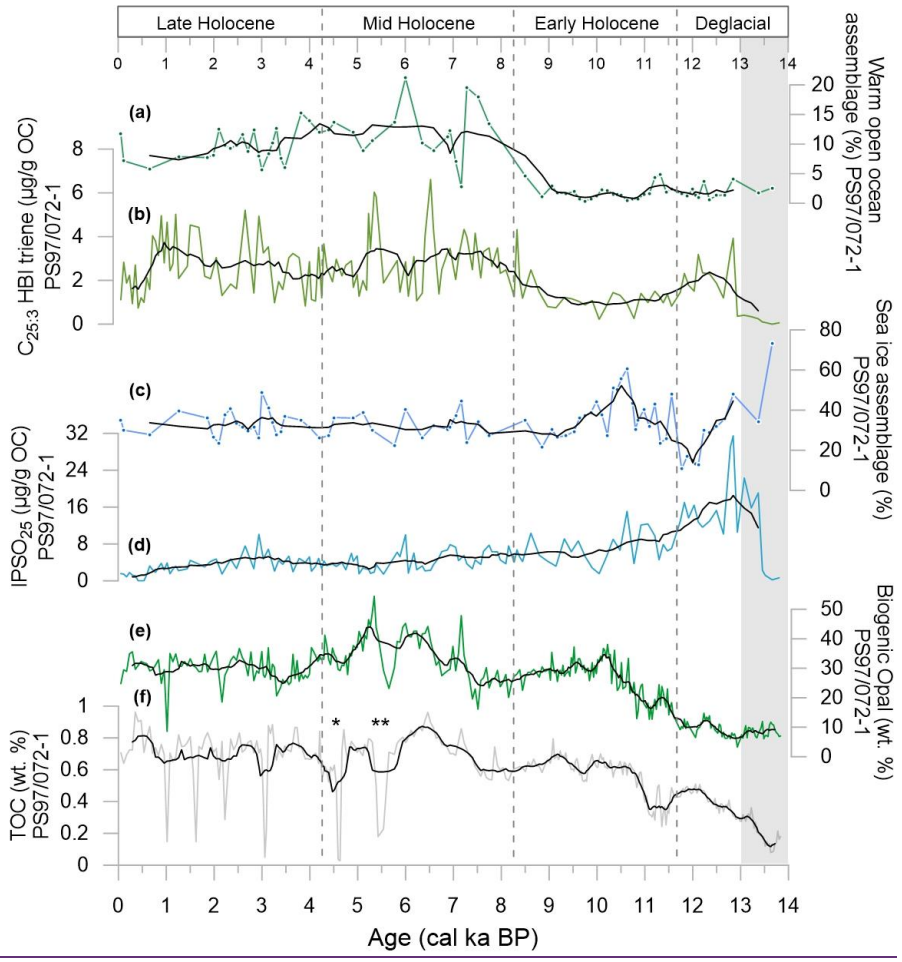
Late Holocene
Mid Holocene
Early Holocene
Deglacial
(a)
(b)
(c)
(d)
(e)
(f)
C25:3 HBI triene (µg/g OC) PS97/072-1
IPSO25 (µg/g OC) PS97/072-1
TOC (wt. %) PS97/072-1
Warm open ocean assemblage (%) PS97/072-1
Sea ice assemblage (%) PS97/072-1
Biogenic Opal (wt. %) PS97/072-1
*
**
Age (cal ka BP)

1151

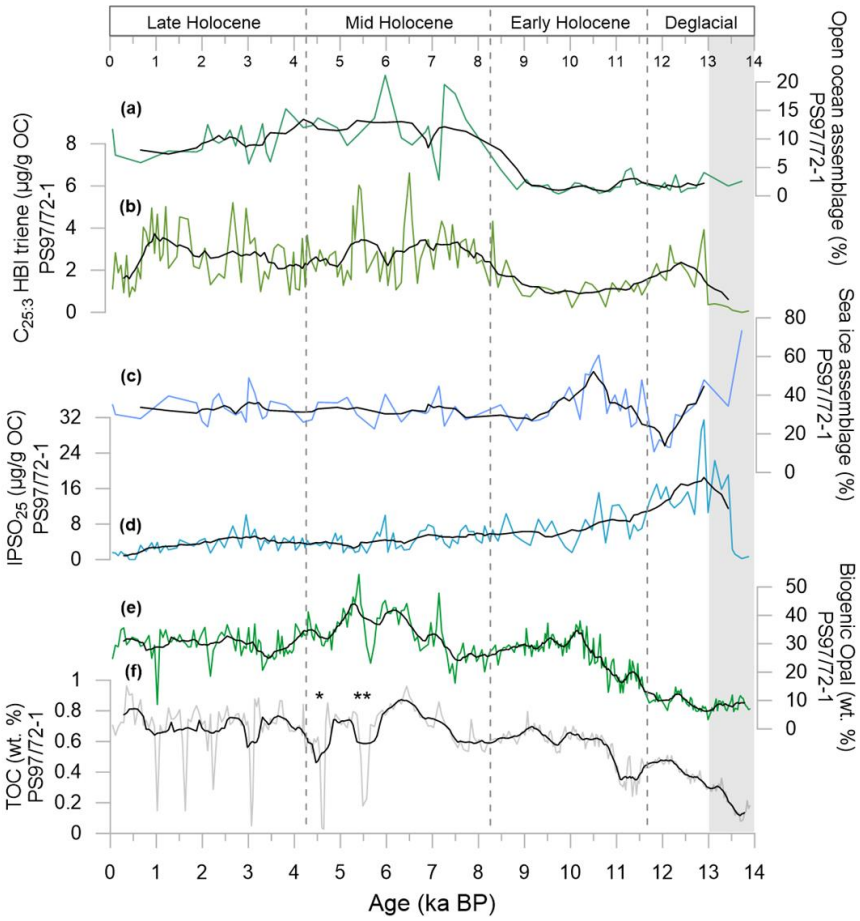

Figure 3: Overview of organic geochemical parameters and main diatom assemblages determined in sediment core PS97/072-1 used to characterize the environmental setting over the past 14 ka BP. a) warm open ocean diatom assemblage, b) $C_{25:3}$ HBI triene, c) sea ice diatom assemblage, d) $IPSO_{25}$, e) biogenic opal and f) TOC contents. Asterisks in f) mark layers of volcanic ash, where ** can be linked to a tephra layer in a sediment core from the Bransfield Strait at 5.5 ka BP (Heroy et al., 2008). Black lines display running averages. Grey shaded interval refers to the Antarctic Cold Reversal.

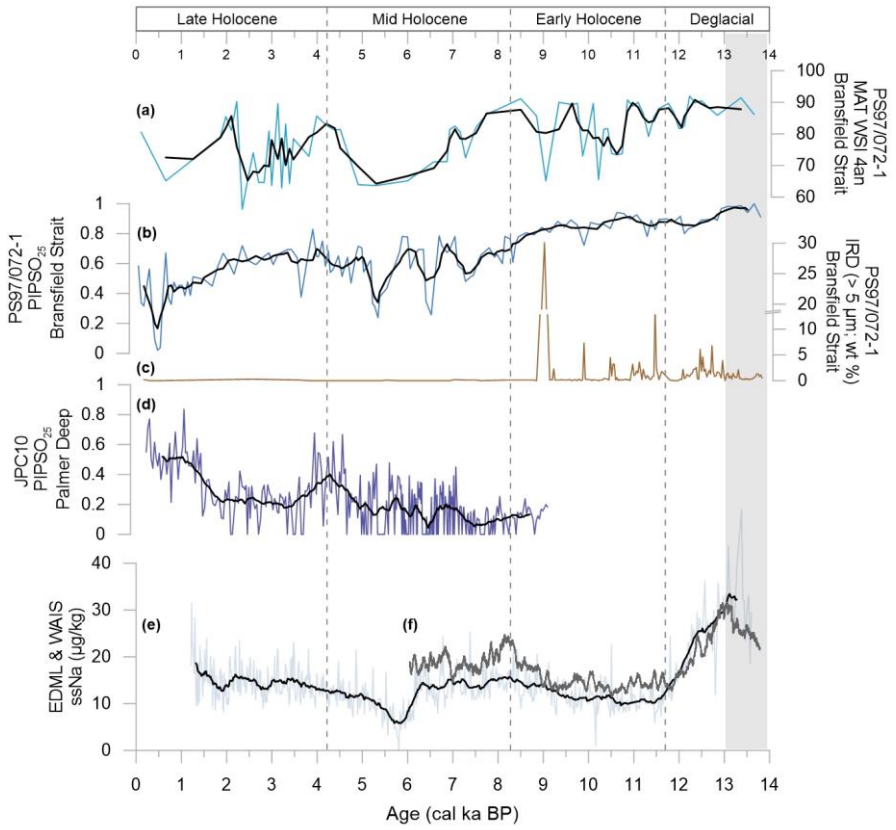
Late Holocene
Mid Holocene
Early Holocene
Deglacial
(a)
(b)
(c)
(d)
(e)
(f)
PS97/072-1 MAT WSI 4an Bransfield Strait
PS97/072-1 PIPSO25 Bransfield Strait
PS97/072-1 IRD (> 5 µm; wt %) Bransfield Strait
JPC10 PIPSO25 Palmer Deep
EDML & WAIS ssNa (µg/kg)
Age (cal ka BP)

1161

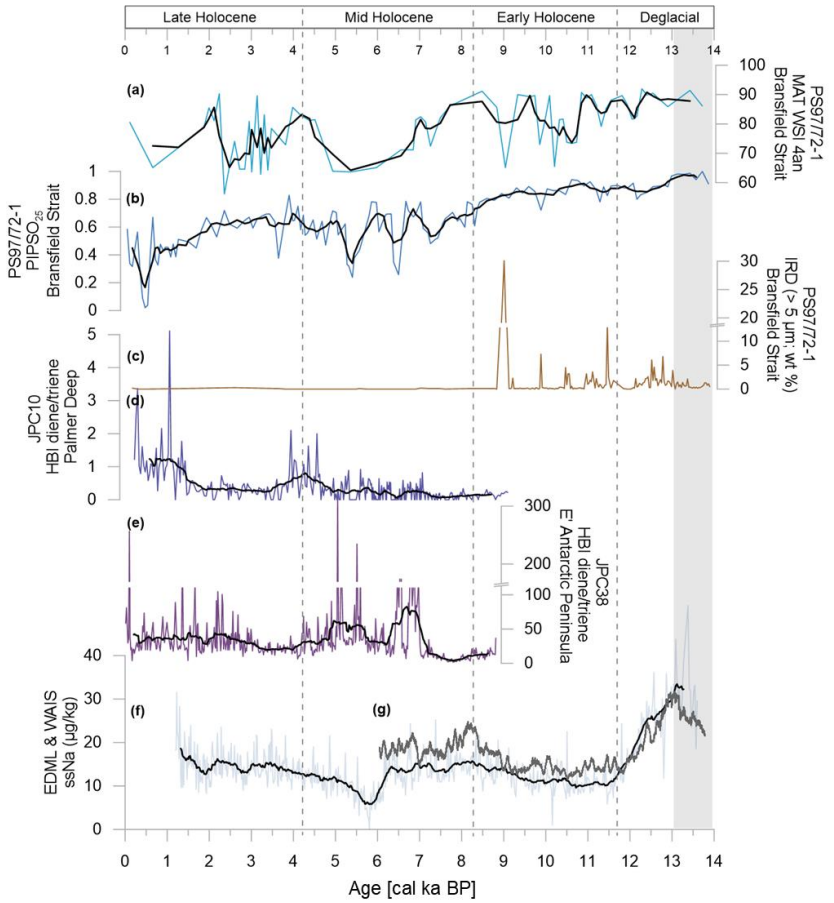

Figure 4: Sea ice related proxies in sediment core PS97/072-1 with a) the diatom based WSI, b) the sea ice index $PIPSO_{25}$, and c) ice rafted debris (IRD). For comparison: $PIPSO_{25}$ values ~~the HBI diene/triene ratio~~ of sediment core d) JPC10 from the Palmer Deep station (Etourneau et al., 2013) and ~~e) JPC38 at the East Antarctic Peninsula (Barbara et al., 2016).~~ ssNa records of e~~f~~) the EDML ice core (Fischer et al., 2007) and f~~g~~) the WAIS ice core (WAIS Divide Project Members, 2015). Black lines display running averages. Grey shaded interval refers to the Antarctic Cold Reversal~~CR~~.

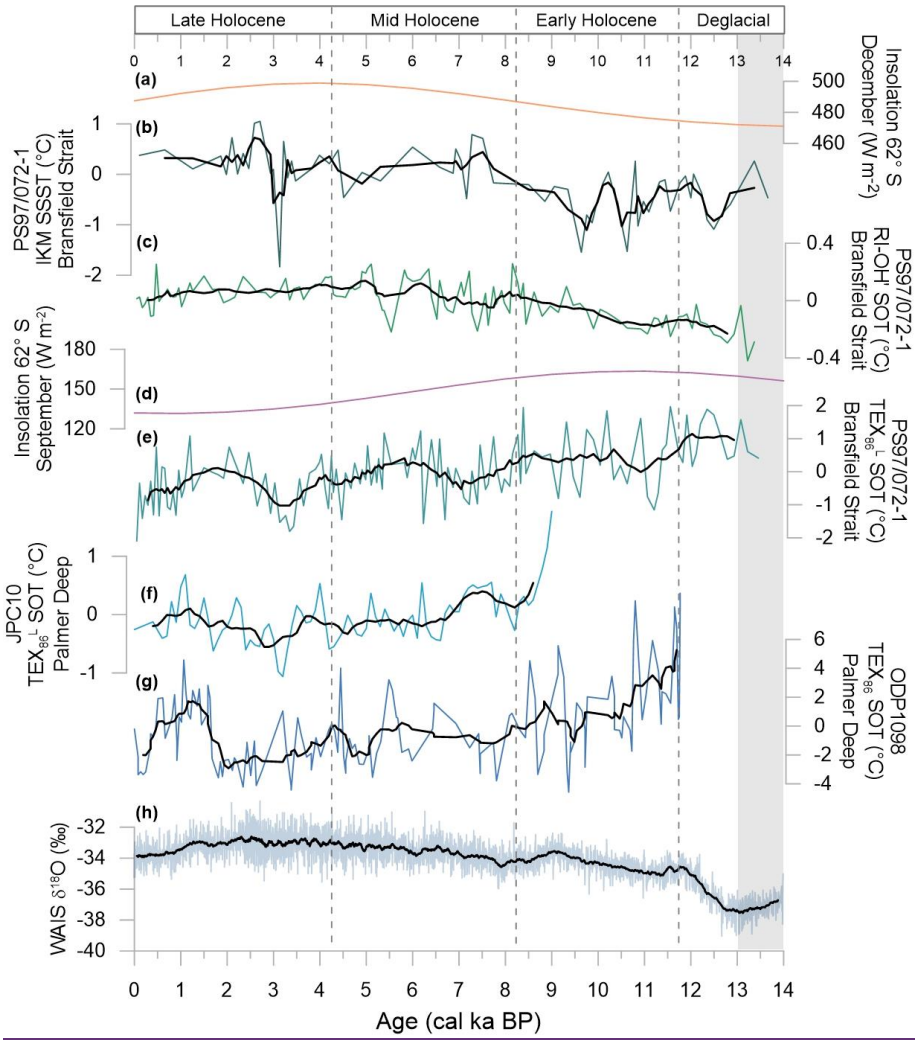
Late Holocene
Mid Holocene
Early Holocene
Deglacial
(a)
(b)
(c)
(d)
(e)
(f)
(g)
(h)
Insolation 62° S December (W m-2)
PS97/072-1 IKM SSST (°C) Bransfield Strait
PS97/072-1 RI-OH' SOT (°C) Bransfield Strait
Insolation 62° S September (W m-2)
PS97/072-1 TEX86L SOT (°C) Bransfield Strait
JPC10 TEX86L SOT (°C) Palmer Deep
ODP1098 TEX86 SOT (°C) Palmer Deep
WAIS δ18O (‰)
Age (cal ka BP)

1171

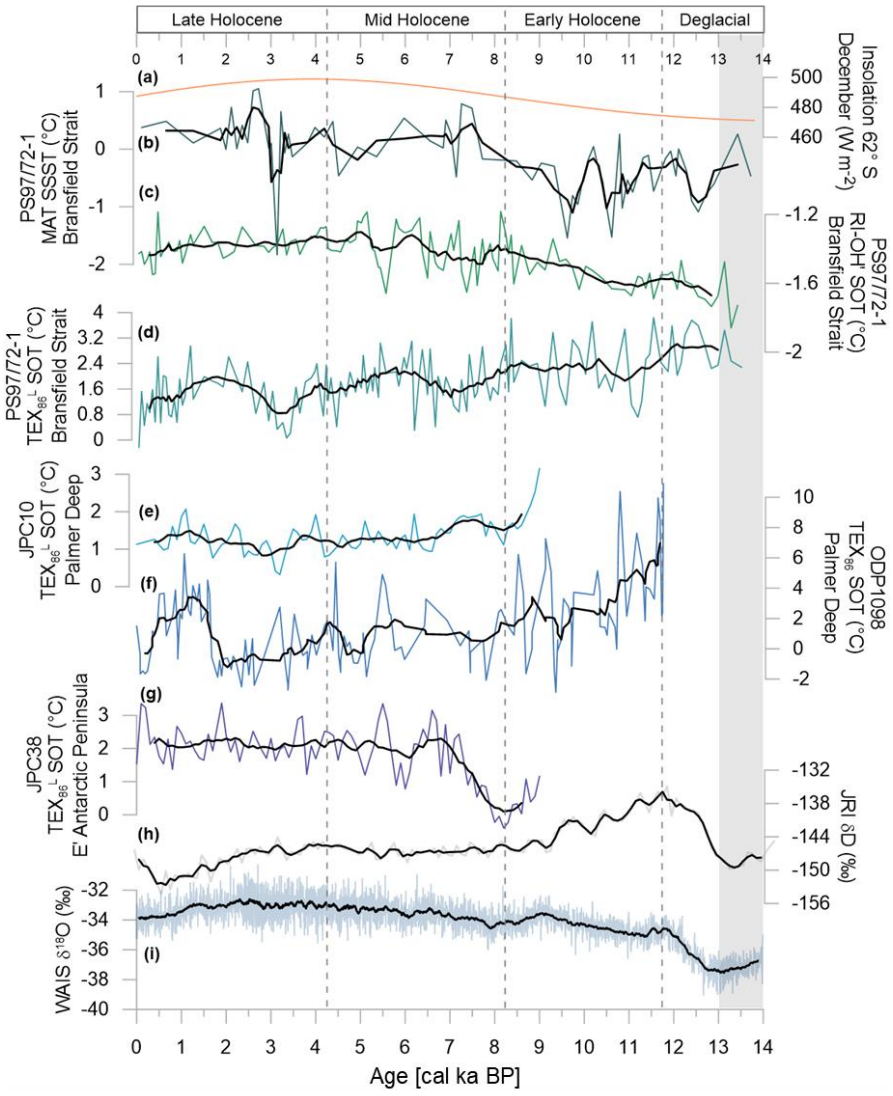

Figure 5: A comparison of a) December insolation (Laskar et al., 2004), b) diatom-based SSST, c) RI-OH'-derived SOT, d) September ~~Spring~~ insolation (Laskar et al., 2004), e) TEX_{86}^{L}-SOT of sediment core PS97/072-1, and temperature reconstructions ~~fe~~) TEX_{86}^{L} from JPC10, Palmer Deep (Etourneau et al., 2013), ~~g~~) TEX_{86} from ODP1098, Palmer Deep (Shevenell et al., 2011), ~~e) TEX_{86}^{L} from JPC38, East Antarctic Peninsula,~~ and h) ice core stable isotope records of ~~h) JRI (Mulvaney et al., 2012) and i)~~ WAIS Divide (WAIS Divide Project Members, 2013). Ocean temperatures are displayed as anomalies with respect to the mean of the individual SOT and SSST

Formatiert: Schriftart: Nicht Fett

values of the entire record. Black lines display running averages. Grey shaded area refers to the Antarctic Cold Reversal.

Formatiert: Schriftart: Nicht Fett

Formatiert: Schriftart: Nicht Fett